Structure-Function Relationships in L-Amino Acid Deaminase, a Flavoprotein Belonging to a Novel Class of Biotechnologically Relevant Enzymes

Paolo Motta[‡,1], Gianluca Molla[‡,§,1,2], Loredano Pollegioni[‡,§], Marco Nardini[†,3]

From the [‡]Dipartimento di Biotecnologie e Scienze della Vita, Università degli Studi deII'Insubria, via J. H. Dunant 3, 21100 Varese, Italy, [§]The Protein Factory, Politecnico di Milano and Università degli Studi deII'Insubria, Varese, Italy
[†]Dipartimento di Bioscienze, Università degli Studi di Milano, via Celoria 26, Italy 20133 Milano, Italy

Running title: *Structure-function relationships in L-amino acid deaminase*

[1]These authors contributed equally to this work.
[2]To whom the correspondence should be addressed: Prof. G. Molla, Dipartimento di Biotecnologie e Scienze della Vita, Università degli Studi deII'Insubria, via J. H. Dunant 3, 21100 Varese, Italy, Telephone: ++39 0332 421414; FAX: ++39 0332 421500; E-mail: gianluca.molla@uninsubria.it.
[3]To whom the correspondence should be addressed: Prof. M. Nardini, Dipartimento di Bioscienze, Università degli Studi di Milano, 20133 Milano, Italy, Telephone: ++39 02 50314898; FAX: ++39 02 50314895; E-mail: marco.nardini@unimi.it

Keywords: L-amino acid deaminase, flavoprotein, membrane-bound enzyme, enzyme structure, structure-function, conformational change, protein engineering, X-ray crystallography

ABSTRACT

L-Amino acid deaminase from *Proteus myxofaciens* (PmaLAAD) is a membrane flavoenzyme which catalyzes the deamination of neutral and aromatic L-amino acids into α-keto acids and ammonia. PmaLAAD does not use dioxygen to re-oxidize reduced $FADH_2$ and thus does not produce hydrogen peroxide; instead, it uses cytochrome b-like protein as electron acceptor. Although the overall fold of this enzyme resembles that of known amine or amino acid oxidases, it shows specific structural features: an additional, novel α+β subdomain placed close to the putative transmembrane α-helix and to the active-site entrance, a FAD isoalloxazine ring exposed to solvent, and a large and accessible active site suitable to bind large hydrophobic substrates. In addition, PmaLAAD requires substrate-induced conformational changes of part of the active site, in particular Arg316 and Phe318, to achieve the correct geometry for catalysis. These studies are expected to pave the way for rationally improving the versatility of this flavoenzyme, which is critical for biocatalysis of enantiomerically pure amino acids.

A variety of enzymes has been used to prepare chiral pharmaceutical and agricultural compounds containing enantiomeric amine or amino acid groups. Among these are aminotransferases (AT, EC 2.6.4.X), lipases (EC 3.1.1.X), amine oxidases (EC 1.4.3.22), amino acid dehydrogenases (EC 1.4.1.X) and amino acid oxidases (EC 1.4.3.X) (1,2).

The deracemization of a racemic amino acid to obtain the L-configuration was achieved by using a stereoselective D-amino acid oxidase (DAAO, EC 1.4.3.3) followed by chemical reduction. The second step iteratively converts the imino acid produced (from the D-amino acid) back into a D,L-mixture to obtain the full resolution of the racemic mixture into the L-enantiomer (1). This approach requires stable recombinant DAAOs possessing wide substrate specificity as well as variants engineered to act on synthetic amino acids (3).

Amino acid oxidases with reverse stereoselectivity are also well-known flavooxidases, mainly produced by snakes or by microorganisms. In particular, L-amino acid oxidases (LAAO, EC 1.4.3.2) catalyze the stereoselective oxidative deamination of L-amino acids into the corresponding α-keto acids and ammonia: the re-oxidation of $FADH_2$ by dioxygen then generates H_2O_2 (4). These flavoenzymes catalyze an irreversible reaction (differently from AT) and do not require a specific step of cofactor regeneration, as otherwise required by the NAD-dependent dehydrogenases. However, owing to the problems associated with overexpression of snake venom LAAOs in

recombinant hosts and the limited substrate acceptance of the microbial counterparts, no appropriate LAAOs for biocatalysis are available (4).

L-amino acid deaminases (LAADs) represent a suitable alternative to LAAOs. LAAD (first identified in the genera *Proteus*, *Providencia* and *Morganella*) catalyzes the deamination of L-isomer of amino acids, yielding the corresponding α-keto acids and ammonia without any evidence of H_2O_2 production. LAAD from *Proteus myxofaciens* (PmaLAAD), expressed in the *E. coli* K12 strain, shows a preference for L-amino acids containing aliphatic, aromatic and sulphur-containing side chains (5). Although the reaction catalyzed by LAAD is of both scientific and practical interest (5-7), no details about its structural-functional relationships and biological significance have been reported so far.

In order to gain more insight into the properties of LAAD, we expressed the *P. myxofaciens* enzyme in *E. coli* and demonstrated that it is a membrane flavoenzyme employing a cytochrome b-like protein as electron acceptor. By using protein engineering studies we were able to produce a truncated, soluble form (PmaLAAD-01N), which was crystallized. Its structural and biochemical characterization clearly shows that LAAD does not belong to the LAAO subfamily of flavo-oxidases, and is characterized by a large and open active site. These studies will provide the strong background needed to rationally alter the versatility of this flavoenzyme: engineered LAAD variants will represent the key to novel applications within the field of amino acids biocatalysis.

EXPERIMENTAL PROCEDURES

Cloning of PmaLAAD Wild-type and Variants—The gene encoding for LAAD from *Proteus myxofaciens* (newly classified as *Cosenzaea myxofaciens*) (8) cloned into the *NdeI* and *Sal*I restriction sites of the pET21a expression plasmid (Merck) was a generous gift from Wolfgang Kroutil (University of Graz, Austria).

PmaLAAD-00N, -01N, -02N and -00C variants (Fig. 1) were produced by PCR. PmaLAAD wild-type gene was amplified using the upstream primers Var00-UP (5'-TAGGCTAGCAACATTTCAAGGAGAAAGCTAC-3'), Var01-UP (5'-TAGGCTAGCATGGTTCGCCGTGATGGTAAA-3') or VAR02-UP (5'-ATTGCTAGCGCCCTGCCATCAGAATCTGATG-3') or VAR00C-UP (5'-TAGCATATGAACATTTCAAGGAGAAAGCTAC-3'); as downstream primer, the primer Var00-DN (5'-GCACGGATCCTTATTACTTCTTAAAACGATCCAAACTAAACGG-3') was used for the -00N, -01N and -02N mutants and VAR00C-DN (5'-CGCACCTCGAGCTTCTTAAAACGATCCAAAC-3') for the -00C mutant. The primers were designed to insert a *NheI* restriction site at the 5'-end and a *BamHI* restriction site at the 3'-end of the amplification products for PmaLAAD-00N, -01N and -02N, and a *NdeI* site at the 5'-end and a *BamHI* site at the 3'-end of the amplification product for PmaLAAD-00C. The amplification products (Pma-VAR00, -VAR01 and -VAR02 genes) were subcloned into the *Nhe*I and *BamH*I restriction sites of the pET11a-His vector (a modified pET11a vector encoding a 6xHisTag sequence which is added at the N-terminus of the recombinant protein) (9), generating the pET11a-His-PMA00, pET11a-His-PMA01 and pET11a-His-PMA02 plasmids. Similarly, the pET24b plasmid was used to generate the pET24b-PMA00C-His expression plasmid by using the *NdeI* and *XhoI* restriction sites. The expressed proteins possess a HisTag sequence (Fig. 1). The sequences of the cloned genes were confirmed by gene sequencing.

Screening of Expression Conditions for PmaLAAD Wild-type and Variants—Expression conditions for PmaLAAD and its variants were screened by a simplified 96-well microplate factorial design approach (10). Four different *E. coli* strains (*E. coli* BL21(DE3), BL21(DE3)pLysS, Origami2(DE3) and Rosetta2(DE3)pLysS strains - Novagen) and two media (LB or modified TB, to which 10 g/L glycerol was added) were used. After overnight incubation at 28 °C, protein expression was induced by adding 0.005 or 0.1 mM final concentration of IPTG. Cells were collected after 4 h (at 28 °C) or 20 h (at 15 °C). PmaLAAD expression was assessed by Western blot analysis using anti-HisTag antibodies (Santa Cruz Biotechnology, Santa Cruz, CA), as well as by activity assay on cell lysates by employing the spectrophometric assay (see below).

Expression and Purification of PmaLAAD Wild-type and Variants—Recombinant wild-type and variants of PmaLAAD were expressed in *E. coli* BL21(DE3) strain under the following

conditions: cells (from a single colony) were grown in modified TB medium containing 10 g/L glycerol, to which 100 μg/mL ampicillin was added (or 30 μg/mL kanamycin for PmaLAAD-00C). Protein expression was induced by adding 0.1 mM IPTG at an OD_{600nm} = 0.5; after 4 hours of growth at 28 °C, cells were harvested by centrifugation.

E. coli recombinant cells expressing PmaLAAD variants were disrupted by sonication in lysis buffer (50 mM potassium phosphate, pH 7.0, 5 mM $MgCl_2$). The cell lysate was separated from the cell debris by centrifugation at 38,500 *g* for 1 h yielding the insoluble fraction of the cell lysate and the crude extract containing the soluble proteins and membrane fragments. For wild-type PmaLAAD, ultracentrifugation of the latter fraction at 150,000 *g* for 2 h produced a membrane fraction (pellet) and a cytoplasmic fraction (supernatant). The membrane fraction was re-suspended in 2.5 mL of 50 mM potassium phosphate, pH 7.0, stored at -80 °C, then thawed and diluted 5-fold in 20 mM triethanolamine-HCl, pH 7.5: centrifugation at 16,000 *g* for 10 min yielded two phases at different density; see Fig. 2 for details.

Recombinant PmaLAAD-00N, -00C and -01N variants from the soluble fraction of the lysates (crude extract) were purified by using metal-affinity chromatography on a HiTrap chelating column (5 mL, GE Healthcare, Little Chalfont, United Kingdom) using 50 mM potassium phosphate buffer, pH 7.5. In the case of PmaLAAD-01N, contaminant proteins bound to the column were eluted with two steps at 25 and 80 mM imidazole, while the variant was eluted at 200 mM imidazole. For crystallographic studies, the purity of PmaLAAD-01N was increased by loading the purified protein (13.7 mg/mL) onto a second HiTrap chelating column (1 mL): elution was performed using increasing concentrations of imidazole (25, 50, 125 and 500 mM).

PmaLAAD-00N and -01N were analysed by size-exclusion chromatography using a Superdex 200 Increase 10/300 column (GE Healthcare).

Activity Assay—The activity on L-Phe was assayed spectrophotometrically by following the formation of the product phenylpyruvate at 321 nm, a wavelength at which the extinction coefficient of the substrate is negligible (5). The protein sample was added to 2 mL (final volume) of 25 mM L-Phe in 50 mM potassium phosphate buffer, pH 7.5, and incubated for 2 min at 25 °C. Every 30 s an aliquot of 400 μL was transferred into a plastic cuvette containing 400 μL of 3 N NaOH to stop the reaction and allow colour to develop. One enzymatic unit corresponds to the amount of enzyme that converts 1 μmol of L-Phe per minute.

Apparent K_m, k_{cat} and V_{max} values for L-Phe were determined by the phenylpyruvate production assay using increasing substrate concentrations, at 25 °C and oxygen air saturation (0.253 mM).

The same assay was used to investigate the ability of commercial quinones (anthraquinone-2,6-disulphonate, anthraquinone-1,5-disulphonate, 2-hydroxy-1,4-naphtoquinone, menadione, duroquinone and juglone), using phenazine methosulphate as mediator, or artificial electron acceptors (indigotetrasulphonate, gallocyanine, 2,6-dichlorophenolindophenol / phenazine methosulphate, cytochrome c and nitroblue tetrazolium) to stimulate the activity of PmaLAAD-00N in the absence of membranes. All compounds were used at 50 μM final concentration, the only exception being phenazine methosulphate which was used at 800 μM final concentration.

The activity of PmaLAAD on L-Phe in the presence of exogenous membranes prepared from *E. coli*, *Streptomyces venezuelae* and human glioblastoma T98G cells was investigated using the spectrophotometric assay.

The deamination reaction of PmaLAAD on L-amino acids in the presence of commercially available *E. coli* lipid extracts (Avanti Polar Lipids, Alabaster, AL) was investigated by means of a polarographic method based on an oxygen electrode (O_2-consumption) assay (11). This assay couples the re-oxidation of the reduced flavin in PmaLAAD with an electron acceptor system that, in turn, consumes dioxygen (see Results section for details). This assay was also employed to investigate the substrate specificity of PmaLAAD on a number of L-amino acids.

Determining optimal pH and Temperature—To investigate the pH dependence of the initial rate of phenylpyruvate production, wild-type PmaLAAD enzymatic activity was assayed at different pH values on 25 mM L-Phe in a multicomponent buffer (160 mM Tris–HCl, 160 mM Na_2CO_3, 160 mM H_3PO_4, 650 mM KCl and 1% glycerol) (12). Data points were fitted based on the equation for two dissociations: $Y = a + b(10^{pH-pKa1}) / (1 + 10^{pH-pKa1}) + [b - c(10^{pH-pKa2}) / (1 + 10^{pH-pKa2})]$ (12).

Temperature dependence of PmaLAAD activity was assayed by measuring the production of phenylpyruvate as described above at different

temperatures, in 50 mM potassium phosphate, pH 7.5, using 25 mM L-Phe as substrate.

Spectral Measurements—Absorbance spectra in the UV–visible region of PmaLAAD variants, as well as ligand-binding experiments, were recorded using a Jasco V-560 spectrophotometer (Jasco Europe, Cremello, Italy) as previously reported (13).

Anaerobic samples were prepared in anaerobic cuvettes by applying ten cycles of evacuation and then flushing with oxygen-free argon. Flavin reduction was carried out by adding 25 mM (final concentrations) of the substrate L-Phe to samples containing ≈ 15 μM enzyme; reduction of the cofactor for PmaLAAD-00N variant was performed both in the absence and in the presence of *E. coli* membranes.

Photoreduction experiments were carried out at 4 °C using an anaerobic cuvette containing 18.5 μM PmaLAAD-00N or 13.1 μM PmaLAAD-01N, 5 mM EDTA and 0.5 μM 5-deaza FAD. The solution was photoreduced using a 250-W lamp and the progress of the reaction was monitored spectrophotometrically (13,14). At the end of the reaction, FAD cofactor was re-oxidized anaerobically by adding 5.5 μM (final concentration) benzyl viologen or by flushing O_2. Photoreduction experiments for PmaLAAD-00N were also performed in the presence of *E. coli* membranes.

Binding experiments of carboxylic acids and sulphite to PmaLAAD-00N and -01N variants were performed by adding small volumes (5 – 50 μL) of concentrated stock solutions (0.1 mM – 1 M) to samples containing 0.8 mL of ≈ 15 μM enzyme and following the changes in the visible absorbance spectrum of the flavin cofactor (13,14).

Far-UV CD spectra of PmaLAAD-00N and -01N variants were recorded using a Jasco J-815 spectropolarimeter equipped with a software-driven Peltier-based temperature controller: the cell path was 0.1 cm (15).

All spectral measurements were recorded at 15 °C in 50 mM potassium phosphate buffer, pH 7.5, except where stated otherwise.

Crystallization, Structure Determination and Refinement—Crystallization trials of PmaLAAD-01N (≈ 10 mg/mL) were performed using the sitting-drop vapour diffusion method with an Oryx-8 crystallization robot (Douglas Instr., East Garston, UK). After a week at 4 °C, crystals were observed under the following growth conditions: 15% PEG 6K, 0.1 M MES (pH 6.5), 10% MPD. They were cryoprotected in a stabilizing solution (20% PEG 6K, 0.1 M MES, pH 6.5, 10% MPD) supplemented with 15% glycerol, and flash-cooled in liquid nitrogen. A single crystal, belonging to the monoclinic space group $P2_1$, diffracted up to 2.0 Å resolution. Diffraction data were collected at the ESRF beamline ID23-2 (Grenoble, France) and processed with XDS (16) and SCALA (17).

The PmaLAAD-01N structure was solved by molecular replacement using the program Phaser (18), with the β-subunit of sarcosine oxidase from *Pseudomonas maltophilia* (PDB code 2GAG) (19) as a search model. Two protein molecules (A and B chains) were located in the crystal asymmetric unit and were subjected to rigid-body and restrained refinement using Phenix (20). The amino acid sequence of the model was modified to match the correct sequence and manually fitted to the electron density using the program Coot (21). A set of restrained refinement cycles were performed using the programs Phenix (20) and Refmac (22). The final refined PmaLAAD-01N structure (R_{factor} = 17.7%, R_{free} = 20.9%) contains 2x447 protein residues (28-474), 2 FAD co-factors, and 518 water molecules, with good stereochemical parameters. Poor electron density is only present at the N- and C-terminus (residues 28 and 474 of both A and B chains).

For soaking experiments and data collection, native PmaLAAD-01N crystals were removed from the crystallization drop with a nylon loop and soaked overnight in a mixture of their stabilizing solution (see above) supplemented with 20 mM anthranilate. The soaked crystals were quickly pulled through a drop of cryoprotectant before being flash-cooled in liquid nitrogen. A single crystal, belonging to monoclinic space group $P2_1$, diffracted up to 1.75 Å resolution (data collection and processing as above).

The structure of the PmaLAAD-01N/anthranilate complex was determined by molecular replacement using the program Phaser (18), with the structure of PmaLAAD-01N as a search model. Two protein molecules were located in the crystal asymmetric unit (A and B chains). The structure was then remodelled with Coot (21) and subjected to restrained refinement, with anisotropic B-factors, using the program Refmac (22). After a few cycles of refinement, the 2Fo-Fc electron density map showed structural details that allowed unambiguous modelling of the bound substrate analogue. The final model (R_{factor} = 15.6%, R_{free} = 19.7%) contains 2x447 protein residues (28-474), 2 FAD cofactors, 2

anthranilate molecules, and 546 water molecules, with good stereochemical parameters. Poor electron density is present at the 28-31 and 337-342 regions and at the C-terminus (residue 474) of both A and B chains.

All data reduction and refinement statistics for both protein models (PmaLAAD-01N and PmaLAAD-01N/anthranilate complex) are reported in detail in Table 1. The stereochemical quality of the models was assessed with MolProbity (23).

The atomic co-ordinates and structure factors for PmaLAAD-01N and PmaLAAD-01N/anthranilate complex (codes 5FJM, 5FJN respectively) have been deposited in the Protein Data Bank (http://www.wwpdb.org/).

Phylogenetic Analyses—Proteins homologous to PmaLAAD were identified with HMMER web server (24) using the "Representative Proteomes" database (25). Sequences sharing an identity > 90% with PmaLAAD were filtered using CD-HIT Suite (26). In addition, amino acid sequences possessing an identity with PmaLAAD < 28% were discarded. Alignment was performed using the MUSCLE algorithm in SeaView software (27). Maximum-likelihood phylogenetic (ML) tree of LAAD sequences was built using PhyML 3.0 server (28). Confidence of branching patterns was assessed by bootstrapping (100 boostrap samples were used) (29). The resulting ML tree was visualized in FigTree v1.4.2 (http://tree.bio.ed.ac.uk/software/figtree/).

RESULTS

Purification of Recombinant Wild-type PmaLAAD—Recombinant PmaLAAD (the sequence of which is reported in Fig. 1*B*) was expressed in *E. coli* BL21(DE3) cells. After cell lysis by sonication and centrifugation, the PmaLAAD activity was fully recovered in the crude extract, as assayed by following the absorbance change at 321 nm due to the conversion of L-Phe into phenylpyruvic acid. After ultracentrifugation of the crude extract, the recombinant enzyme was mainly associated to the membrane fraction (*i.e.* in the pellet fraction) which was re-suspended in 50 mM potassium phosphate buffer, pH 7.5, obtaining a ≈ 2-fold increase in specific activity (Fig. 2).

Interestingly, thawing, diluting (5-fold) in 20 mM triethanolamine-HCl, pH 7.5, and centrifuging the membrane fraction stored at -80 °C resulted in a phase separation: the lower, denser phase contained about half of the PmaLAAD of the sample (based on the enzymatic activity and SDS-PAGE analysis) and showed a further ≈ 2.5-fold increase in specific activity, reaching 2.9 U/mg of protein, with an overall yield of 33% (Fig. 2). Based on the purity degree (29%, see lane 7 in Fig. 2B, left panel), a k_{cat} = 8.5 s^{-1} was estimated. Owing to the failure to produce a soluble, membrane-free preparation of wild-type PmaLAAD, chromatographic steps were not effective in purifying enzyme.

In addition, N- and C-terminal His-tagged full-length proteins were produced (PmaLAAD-00N and -00C, respectively, Fig. 1) and expressed at a level similar to that of wild-type PmaLAAD by using BL21(DE3) or Origami *E. coli* strains. When the crude extract containing PmaLAAD-00N (specific activity on L-Phe of 0.8 U/mg protein) was loaded on a HiTrap chelating column it separated into two fractions: the flow-through containing the active enzyme (≈ 500 U/L fermentation broth, 90% of purification yield) associated to membrane fragments, and the fraction eluted at 0.2 M imidazole which contained a significant part of PmaLAAD-00N (devoid of membranes). Following dialysis to eliminate imidazole, the latter fraction showed a purity degree ≥ 90% (as estimated by SDS-PAGE analysis, lane 5 in Fig. 2*B*, central panel) and was fully stable (see spectral properties, below). However, the measured LAAD activity was only marginal (5 U/L fermentation broth); therefore, this fraction was named "quasi-inactive" PmaLAAD-00N. Similar results were obtained for the PmaLAAD-00C variant: again, after loading on the HiTrap chelating column, enzymatic activity was detected mainly in the flow-through fraction (≈ 250 U/L fermentation broth), while the fraction eluted at 0.5 M imidazole contained a significant part of PmaLAAD-00C protein but showed only marginal LAAD activity (< 2%), and a purity of ≈ 70% (as estimated by SDS-PAGE analysis), not shown.

Biochemical Properties of Partially Purified, Membrane-bound PmaLAAD—The specific activity of PmaLAAD in the crude extract, which contains membranes, on 25 mM L-Phe as substrate was ≈ 0.6 U/mg protein (assayed as production of phenylpyruvic acid). The dependence of the initial rate on L-Phe concentration is shown in Fig. 3*A*: the $K_{m,app}$ = 3.27 ± 0.96 mM and $V_{max,app}$ = 1.35 ± 0.08 U/mg protein values are in good agreement with those

reported in the literature ($K_{m,app}$ = 2.3 mM, $V_{max,app}$ = 2 U/mg) (5). As a result of the 12% purity degree of PmaLAAD in the crude extract, a k_{cat} = 8.3 s^{-1} was estimated. No substrate inhibition was evident up to 100 mM L-Phe. On the same enzyme preparation, the activity on L-Phe was also assayed as O_2 consumption (*i.e.* by polarographic assay) (11), yielding an identical specific activity.

From this evidence we conclude that the membrane-containing PmaLAAD preparation catalyzes the O_2-dependent oxidative deamination of L-Phe.

By employing the O_2-consumption assay we investigated the relative substrate specificity of PmaLAAD toward natural and synthetic amino acids: the polarographic assay was carried out using a fixed volume of membrane-associated PmaLAAD (corresponding to ≈ 0.5 mg of total membrane proteins) and 25 mM substrate concentration. As shown in Table 2, PmaLAAD is specific for aromatic, neutral L-amino acids; a low activity was assayed towards small, charged or polar L-amino acids. Notably, a significant activity was also measured on the synthetic amino acid L-phenylalanine ethylester (whose α-carboxylic group is esterified) and on L-DOPA (33% and 56.7% in comparison to L-Phe, respectively). No significant activity was assayed with D-amino acids (Table 2).

The pH dependence of PmaLAAD activity was evaluated on the sample from the membrane fraction by using the spectrophotometric assay in the 3 to 10 pH range (12). The highest activity is apparent at neutral pH (between 7 and 7.5) and is negligible below pH 5 and above pH 9 (Fig. 3*B*). Concerning the temperature dependence, the activity of PmaLAAD linearly increased up to 50 °C and then rapidly decreased, becoming negligible at 70 °C (Fig. 3*C*). This behaviour resembles that reported for LAAD from *P. mirabilis* (optimal temperature of 45 °C) (30).

Notably, PmaLAAD in the crude extract showed a fairly good stability since it showed a 50% residual activity after 24 hours of incubation at 25 °C. The enzyme retained ≈ 50% and ≈ 75% of the original activity when stored for 1 month in the presence of 10% glycerol at -20 °C and at -80 °C (even without glycerol), respectively.

Overall, the properties of this PmaLAAD preparation seem to satisfy the requirements for application in biocatalysis of natural and unnatural amino acids (2).

Biological Activity of PmaLAAD: Effect of Membranes—The enzymatic activity (assayed as production of phenylpyruvic acid) of purified, membrane-free, quasi-inactive PmaLAAD-00N is very low (see above): notably, it was significantly enhanced by adding *E. coli* membranes and sonication. Actually, the addition of an amount of membranes from *E. coli* cells (not expressing PmaLAAD) corresponding to ≈ 0.30 mg of cells for each μg of enzyme increased the PmaLAAD-00N activity by ≈ 50-fold. No further increase in enzymatic activity was obtained using larger amounts of membranes. As a control, sonication of PmaLAAD-00N in the absence of exogenous membranes resulted in a 6-fold decrease in the original, low enzymatic activity. Notably, recovery of PmaLAAD activity depended on the membrane's source: no recovery of the enzymatic activity was observed using membranes from the micro-organism *Streptomyces venezuelae* while a low, partial recovery was apparent (2.7-fold) using membranes from human glioblastoma T98G cells. Similarly to PmaLAAD-00N, a ≈ 32-fold increase in enzymatic activity was apparent by adding *E. coli* membranes prepared from 2.25 mg cells, to 75 μg of purified PmaLAAD-00C.

The dependence of PmaLAAD-00N activity on a putative molecular partner associated to the bacterial membrane was investigated by mixing the purified enzyme variant with two commercially available *E. coli* lipid extracts (Avanti Polar Lipids). Mixing 150 μg of PmaLAAD-00N with 4.5 mg of Total Lipid extract (containing 17.6% unknown components, mainly lipoproteins) resulted in a slight (4-fold) increase in activity, which is significantly lower than the activity recovery observed using the same amount of *E. coli* membranes (= 32-fold). Employing the Polar Lipid extract (with a higher degree of purity) an even lower increase in enzymatic activity was apparent (1.6-fold, Table 3). To exclude any inhibitory effect of a component of the lipid extracts, 150 μg of PmaLAAD-00N were mixed with 2.25 mg of lipid extract and a corresponding amount of *E. coli* membranes (22.5 mg): the recovery of the enzymatic activity resembled the value observed for *E. coli* membranes only.

Altogether, these results suggest that a specific membrane partner(s) -- which is(are) available in *E. coli* membrane preparations -- is required for the purified, quasi-inactive PmaLAAD-00N to recover the enzymatic activity. Membranes from an unrelated source or a hydrophobic environment, such as the one provided by purified lipid extracts, are not suitable for recovering PmaLAAD activity.

Spectral Characterization of Purified PmaLAAD-00N—The spectral properties were assessed using the membrane-devoid PmaLAAD-00N variant because of its higher purity compared to the form lacking the HisTag and the absence of membranes affecting the measurements. PmaLAAD-00N shows the canonical absorbance spectrum of FAD-containing flavoproteins with three main peaks at 277, 380 and 456 nm (Fig. 4*A*). The ratio between the absorbance at 277 nm and at 456 nm is ≈ 8.9, and the estimated molar extinction coefficient is 14168 $M^{-1}cm^{-1}$ at 456 nm. The absorbance spectrum of PmaLAAD-00C resembled that of PmaLAAD-00N (data not shown): this indicates that the location of the HisTag does not affect the flavin environment of PmaLAAD. The far-UV circular dichroism spectrum shows that PmaLAAD-00N is folded and contains secondary structure elements (not shown).

Amino acid oxidases are known to interact with a number of carboxylic acids, yielding specific spectral modifications and thus representing useful active-site probes (4,31,32). The binding to PmaLAAD-00N of various compounds known as DAAO and/or LAAO active-site ligands (14,33,34) was investigated in the absence and in the presence of *E. coli* membranes (corresponding to ≈ 0.30 mg of cells for each μg of PmaLAAD-00N). No spectral perturbations were evident up to ≈ 0.4 M sodium benzoate, suggesting that PmaLAAD-00N cannot bind this well-known DAAO ligand (31,35). However, when the same experiment was performed using anthranilate (2-aminobenzoate), specific spectral perturbations were observed in the 400- to 500-nm and in the 520- to 600-nm range (Fig. 4*C*); the latter spectral changes are due to the formation of a charge-transfer complex between the ligand and the FAD cofactor, as observed for other amino acid oxidases (31,35). These absorbance changes were more evident in the absence of membranes: from the absorbance changes at 533 nm as a function of anthranilate concentration, a K_d of 18.4 ± 4.4 mM was calculated (n=3, Fig. 4*C*, inset). The same experiment was performed using kojic acid as ligand (Fig. 4*E*), yielding a general increase in absorbance in the visible region of the spectrum with a saturation behaviour (K_d = 3.0 ± 0.3 mM) (n=3, Fig. 4*E*, inset). Overall, PmaLAAD-00N binds selected carboxylic acids, resulting in specific alterations of the visible spectrum of the flavin cofactor.

We then demonstrated that the flavin cofactor bound to PmaLAAD is catalytically competent. Actually, when the PmaLAAD-00N variant was mixed under anaerobic conditions with an excess of substrate (25 mM L-Phe), the flavin cofactor rapidly reacted with the substrate, yielding the typical absorbance spectrum of the reduced FAD (*i.e.* bleaching of the 450-nm peak in the dead time of mixing for the membrane-free preparation) (Fig. 4*A*). Notably, the time course of flavin reduction was identical under aerobic conditions. We could then establish the reductive half-reaction catalyzed by PmaLAAD:

FAD + L-Phe Δ $FADH_2$ + phenylpyruvic acid (eq. 1)

No spectral perturbations resembling flavin reduction were observed by adding sulphite to PmaLAAD-00N instead (up to ≈ 0.45 M Na_2SO_3), this suggesting divergences in FAD reactivity between PmaLAAD and the enzymes belonging to the oxidase class of flavoproteins (33).

Anaerobic photoreduction of PmaLAAD-00N in the presence of 5 mM EDTA and 0.5 μM 5-deaza-FAD generated the reduced FAD cofactor form after 5 min of exposure to intense light radiation (Fig. 4*G*). A large amount of the anionic semiquinone flavin form was evident, as made apparent by the large increase in a peak at ≈ 380 nm, an effect due to intense light irradiation. A full re-oxidation of membrane-free, fully photoreduced PmaLAAD-00N requiring minutes to completion was observed both by admitting O_2 (see below) than by adding benzyl viologen (Fig. 4*G*).

Formation of the Reduced Form of a Cytochrome b-like Protein During PmaLAAD-00N Reaction in Membranes—The time course of FAD reduction of PmaLAAD-00N in the presence of membranes by an excess of L-Phe under anaerobic conditions was clearly biphasic: a large, rapid decrease at 450 nm was followed by a slower and smaller further decrease (taking ≈ 15 min to completion, Fig. 4*B*). Interestingly, three narrow absorbance peaks are evident following full FAD reduction: one major peak at 429 nm and two minor peaks at 532 nm and 560 nm (Fig. 4*B*). These peaks correspond to the ones typically associated with the reduced form of cytochrome b (36), a small membrane protein usually associated with redox enzymes (37). For details concerning cytochromes in *Proteous* species see (38,39). Notably, when the same reaction was performed under aerobic conditions, the spectrum of the reduced cytochrome was observed only when the L-Phe concentration exceeded the concentration of dissolved O_2 (i.e. at > 0.3 mM L-Phe). These

data demonstrate that in the presence of membranes, L-Phe deamination by PmaLAAD is coupled to reduction of a cytochrome b-like protein.

In the presence of membranes, 1:1 (v/v) ratio corresponding to 30 mg of cells for each μg of enzyme, the rate of flavin photoreduction of PmaLAAD-00N was increased (3.5 min to reach complete reduction, Fig. 4*H*) as compared to the same experiment in the absence of membranes. Notably, the isosbestic point at 410 nm observed in the photoreduction experiment in the absence of membranes was not conserved due to the formation of a Soret band of cytochrome b at 429 nm. In the presence of membranes, too, a large amount of the anionic semiquinone flavin form was evident, as made apparent by the large increase in a peak at ≈ 380 nm due to intense light irradiation.

O_2-Reactivity─The L-Phe deamination activity of PmaLAAD in the presence of membranes is coupled to O_2 consumption (see above). Dioxygen is absolutely required to produce phenylpyruvic acid from L-Phe under these experimental conditions: the rate constant for ketoacid production under anaerobic conditions is ≈ 3% of the value assessed at air saturation. Indeed, the reaction rate did not depend on O_2 concentration since a similar apparent activity was determined at ≥ 10% O_2-saturation.

Known LAAO and DAAO flavoenzymes employ O_2 to re-oxidize the reduced $FADH_2$ cofactor yielding H_2O_2. Notably, when using wild-type PmaLAAD in the crude extract, which is associated to membranes, no halving of oxygen consumption was observed by adding a large excess of catalase, which converts H_2O_2 into H_2O and ½ O_2, to the reaction mixture of the polarographic assay, this demonstrating that no H_2O_2 was produced during the enzymatic reaction. Lack of H_2O_2 production was also confirmed by the classic *o*-dianisidine/peroxidase spectrophotometric, coupled assay used for flavoprotein oxidases (11). Similarly, no superoxide was produced by the PmaLAAD reaction since the O_2 consumption was not modified by adding up to 24 U of superoxide dismutase.

Opening the cuvette containing fully photoreduced membrane-devoid PmaLAAD-00N to air, conversion into the fully re-oxidized flavin spectrum required ≈ 20 min, showing a very limited dioxygen reactivity of reduced PmaLAAD-00N (k_{reox} ≤ 0.08 s^{-1}). Mixing the photoreduced membrane-devoid PmaLAAD-00N with buffer solutions equilibrated at increasing O_2 concentrations in the stopped-flow device (5-50% oxygen saturation, final concentration) did not yield the re-oxidized form of the flavin cofactor (33) during the measurement (≈ 2 min), as otherwise normally observed for flavo-oxidases.

Altogether, these results demonstrate that the flavin molecule bound to PmaLAAD is quickly reduced by the substrate but it is not efficiently re-oxidized by O_2 since the rate constant is not sufficient for the observed turnover (0.08 vs. ≈ 8 s^{-1}, respectively). The O_2 consumption observed in the presence of membranes is clearly not due to a direct, O_2-induced re-oxidation of the flavin cofactor bound to the enzyme. We suggest that in membranes the reduced flavin form of PmaLAAD is re-oxidized by two oxidized cytochrome b-like proteins:

$$E\text{-}FADH_2 + 2cyt_{ox} \;\Delta\; E\text{-}FAD_{ox} + 2cyt_{red} \quad \text{(eq. 2)}$$

that then transfer the electrons through the respiratory chain to dioxygen yielding H_2O. Actually, using 250 μM antimycin A, an inhibitor of the respiratory chain, the O_2-consumption of L-Phe oxidation by PmaLAAD in resuspended membranes is drastically decreased (≥ 60%).

The activity of purified, membrane-devoid PmaLAAD-00N was also detected using artificial electron acceptors, such as indigotetrasulphonate, gallocyanine, 2,6-dichlorophenolindophenol, cytochrome c and nitroblue tetrazolium. The highest activity was apparent with 2,6-dichlorophenolindophenol /phenazine methosulphate (E_m = 217 mV at pH 7.5): specific activity was 8-fold higher than the value determined with oxygen only. In contrast, a more modest increase in activity (3 to 4-fold) was observed when quinones, such as anthraquinone-2,6-disulphonate, anthraquinone-1,5-disulphonate, 2-hydroxy-1,4-naphtoquinone, menadione, duroquinone and juglone, were used as electron acceptors. Furthermore, adding duroquinone or juglone (50 μM) to the PmaLAAD membrane-containing fraction or to purified PmaLAAD added of Polar Lipid extract (as in Table 3) resulted in a moderate, ≤ 2–fold increase in activity.

Production and Properties of the Soluble PmaLAAD-01N Variant─In order to design a PmaLAAD variant not able to associate to membranes and thus suitable for crystallographic studies, the amino acid sequence of the wild-type protein was analysed using the TMPred server (40). A putative transmembrane α-helix (residues 8 to 27) was predicted in the N-terminal region

(Fig. 1*A*). Based on this prediction, two deletion variants were designed starting from Met28 (PmaLAAD-01N) and Ala50 (PmaLAAD-02N), respectively. Both variants were produced with an additional HisTag sequence at the N-terminus to facilitate their purification (Fig. 1*A*,*B*). The PmaLAAD-02N variant was not characterized because of its low stability.

The PmaLAAD-01N variant, lacking the putative transmembrane α-helix, was expressed by following the same protocol used for PmaLAAD and PmaLAAD-00N and was purified from the crude extract by HiTrap chelating affinity chromatography. PmaLAAD-01N is almost completely soluble: ≈ 25 mg of pure PmaLAAD-01N were purified from 1 L of culture with a > 90% purity (Fig. 2*B*, lane 5 in right panel). The enzymatic activity of the pure PmaLAAD-01N preparation was below detection even when exogenous *E. coli* membranes were added to the assay mixture.

PmaLAAD-01N shows an absorbance spectrum very similar to that of PmaLAAD-00N, with an estimated molar extinction coefficient at 458 nm of 12193 $M^{-1}cm^{-1}$ (Fig. 4*A*). In contrast, the far-UV circular dichroism spectrum of PmaLAAD-01N differs from the one recorded for the PmaLAAD-00N counterpart, showing, as expected, a decrease in α-helix content (not shown).

When analysed by size-exclusion chromatography, purified PmaLAAD-01N eluted in a single peak, corresponding to a molecular mass of 44.6±0.5 kDa (n = 3) kDa (slightly lower than the expected value of 49.9 kDa), thus indicating that it is monomeric in solution in the 1-5 mg/mL protein concentration range. A similar result was obtained for the soluble fraction of full-length PmaLAAD-00N (≈ 47 kDa).

Similar to PmaLAAD-00N, PmaLAAD-01N did not bind benzoate and did not react with sulphite but did interact with anthranilate, yielding a spectral perturbation which resembles a charge-transfer complex (K_d = 36.7 ± 5.6 mM, Fig. 4*D*). PmaLAAD-01N was also titrated with 2-aminobenzaldehyde: binding of this compound resulted in a large spectral change in the 500- to 580-nm range (K_d of 0.31 ± 0.05 mM n=3, Fig. 4*F*).

When purified PmaLAAD-01N was mixed under anaerobic conditions with an excess of substrate (25 mM L-Phe), the FAD cofactor rapidly converted into the reduced form, thus demonstrating that it is catalytically competent. Notably, the time course of flavin reduction and the absorbance spectrum of the reduced enzyme form were identical under both aerobic and anaerobic conditions, pointing to a limited O_2-reactivity of the deleted PmaLAAD variant, too. Photoreduction of the FAD cofactor in PmaLAAD-01N was fully accomplished after ≈ 10 min of illumination (with a large amount of anionic semiquinone formation) and the photoreduced enzyme was reverted to the oxidized form by mixing with benzyl viologen.

Altogether, the spectral, binding and oligomerization properties of the deletion variant PmaLAAD-01N resemble those of the full-length enzyme. The main difference is its inability to associate with membranes, which prevents efficient L-Phe oxidation.

Overall Structure of PmaLAAD-01N—The PmaLAAD-01N was solved at 2.0 Å resolution and refined to final R-factor and R-free of 17.7% and 20.9%, respectively. Data collection and refinement statistics are reported in Table 1. PmaLAAD-01N consists of two domains: a FAD-binding domain (Fbd: residues 40-100, 203-276, 413-474) similar to the glutathione reductase 2 family (41) and a substrate-binding domain (Sbd: residues 28-39, 101-202, 277-412) (Fig. 5*A*).

The Fbd is made up of a six-stranded β-sheet with β10-β3-β2-β14-β24-β23 topology flanked by a helix bundle formed by A1-A3-A6-A14 on one side and by a three-stranded β-sheet β11-β12-β13 and helix A7 on the other side. The C-terminal A15 and A16 helices (3_{10}) run orthogonally to strand β23 (Figs. 5*B,C*). The helices A1 and A14 of the helix bundle pack against the central six-stranded β-sheet with their N-termini directed toward the FAD molecule. Helix A3 forms an outer layer of the fold, running orthogonally behind the A1, A6 and A14 helices. On the same side, the 3_{10} helix A2 flanks the pyrophosphate group of FAD. On the other side, the N-terminus of helix A7 is directed toward the FAD molecule.

The Sbd consists of a mixed, eight-stranded β-sheet with β7-β8-β6-β16-β17-β18-β15-β22 topology and is flanked by helices A4, A5, A12 and the 3_{10} helix A13. The long β15 and β22 strands connect the Sbd and the Fbd, forming a four-stranded mixed β-sheet with β19 and β20. Another connection between the two domains is provided by strands β4 and β9 that form with strand β5 a small, anti-parallel, three-stranded β-sheet (Fig. 5*B*).

The Sbd is characterized by the presence of a long region of 67 amino acids nestled between strand β19 and helix A12: this subdomain shows

an α+β structure whose arrangement is unprecedented, as suggested by a DALI search (42). The α region consists of four helices: A8, A9, A10 and A11; the β-region includes strand β20, which forms a parallel two-stranded β-sheet with β19 from the core of the Sbd, and an anti-parallel two-stranded β-sheet built up by strand β1 and β21. In particular, strand β1 belongs to the N-terminal region of PmaLAAD-01N (residues 28-39), which crosses the subdomain on the protein surface before inserting in the Fbd (Fig. 5*A*,*B*).

Regarding the quaternary assembly, the two PmaLAAD-01N molecules in the crystal asymmetric unit face each other in the Sbd regions corresponding to the end of A3 and the following loop, to A4-β7-A5, to A6 and to β16-β17. The facing residues (25 in each monomer) make six salt bridges and two H-bonds (distances 3-3.5 Å). According to the program PISA (43), these interactions make the complex stable, but the overall buried surface area is modest, ≈ 700 Å^2 for each monomer corresponding to ≈ 4% of the total accessible surface area. Thus, in agreement with size-exclusion chromatography experiments, the PmaLAAD-01N does not show any quaternary architecture and can be considered monomeric.

Structural Relatives─A DALI analysis (42) indicates that the PmaLAAD-01N tertiary structure resembles that of a series of FAD-binding oxidoreductases, such as the β subunit of L-proline dehydrogenase from *Pyrococcus horikoshii* (PDB code 1Y56; DALI Z-score of 42.3, residue identity of 23%) (44), glycine oxidase from *Bacillus subtilis* (PDB code 1C0I; DALI Z-score of 41.2, residue identity of 21%) (45), and the heterotetrameric sarcosine oxidase from *Corynebacterium* sp. U-96. (PDB code 3ADA; DALI Z-score of 40.9, residue identity of 23%) (46) and from *Stenotrophomonas maltophilia* (PDB code 2GAG; DALI Z-score of 40.2, residue identity of 23%) (19) (Table 4).

The structural relationship among all these proteins extends to an excellent conservation of tertiary structure, with a r.m.s. deviation ranging from 2.0 to 2.2 Å. The structural homology is particularly marked for the isolated Fbd, with a r.m.s. deviation in the 1.2- to 1.3-Å range, while for the isolated Sbd it ranges from 1.9 to 2.2 Å (Table 4). Although the general correspondence of secondary structure elements is maintained in both domains (Fig. 5*C*), the orientation of the Sbd is slightly different if the Fdb is used for the structural superimposition (Fig. 6*A*). Most importantly, the additional α+β subdomain present in PmaLAAD-01N (Fig. 5*C*) is absent as such in the other related proteins, with the first 20 N-terminal residues of PmaLAAD-01N either absent in 1Y56 and in 1C0I, or differently oriented if compared to the N-terminal region of 3ADA and 2GAG (Fig. 6*B*). We cannot exclude that the absence of the anchorage N-terminal helix in PmaLAAD-01N, as compared to the full-length enzyme, might affect the conformation of the following region.

FAD Binding Site─FAD binds to PmaLAAD-01N in an extended conformation similar to that found in related FAD-binding proteins (Fig. 7*A*) (41). Forty-three residues are directly involved in FAD binding (distances below 4.5 Å), sixteen of which establish electrostatic or polar interactions with the co-factor. Only five of the latter interactions involve side-chain atoms (residues Glu85, Lys86, Gln93, Ser94, Thr442), the others being due to main-chain atoms. The N-terminal ends of the helix dipole of A14 and of A1 are pointed toward the O2 position of the isoalloxazine ring, and toward the pyrophosphate group of FAD, respectively. These two dipoles are typical of GR2 family members.

Overall, the isoalloxazine ring is quite exposed to solvent, especially at the N5 reactive site, located at the interface between the Fdb and the Sbd. It establishes hydrogen bonds with the N atom of Met441 and the N and OG1 atoms of Thr442 (FAD O2 atom), the N atoms of Ser99 and Gln100 (FAD O4 atom), and the N atom of Tyr98 (FAD N5 atom) while displaying van der Waals interactions with Gln93, Arg96, Ala97, Tyr98, Ser99, Gln100, Leu279, Gln281, Ala410, Val411, Val412, Val438, Trp439, Gly440, Met441, and Thr442 side chains. The FAD O4 atom is further hydrogen bonded to a water molecule located inside the active-site cavity (Fig. 7*B*).

Furthermore, the model of PmaLAAD-01N in complex with N5-sulpho-FAD (generated on the basis of the isoalloxazine ring of a N5-sulpho-flavin mononucleotide, PDB code 1QCW) shows that the close vicinity of the PmaLAAD-01N helical A2 segment to the FAD N5 reactive site would provide steric clash of the bound sulphite with the A2-β4 loop (Fig. 7*C*), thus preventing sulphite binding (see above). In addition, the lack of such a peculiar feature of the flavo-oxidases is also supported by the absence of positively charged groups in proximity of the N1-C2=O locus of the isoalloxazine ring, whose presence would inductively promote the process: in PmaLAAD a partial positive charge may be only

provided by the dipole associated to the N-terminus of the nearby helix A14.

Substrate Binding Site—In order to gain structural insight into the substrate-binding mode of the enzyme, the structure of PmaLAAD-01N in complex with anthranilate (possessing both a carboxyl and an amino group, thus mimicking L-amino acids) was determined at 1.75 Å resolution (R_{factor} = 15.6%, R_{free} = 19.7%). Data collection and refinement statistics are reported in Table 1. The analysis of the calculated electron density map showed the substrate-analogue bond near the FAD isoalloxazine moiety (Fig. 8*A*).

Binding of anthranilate does not alter the PmaLAAD-01N global tertiary structure (r.m.s. deviation range 0.43-0.59 Å between complex and native structures, depending on the superimposed protein chains), nor promote quaternary assembly variation. Local differences in the backbone conformation are, however, evident in the β18-β19 loop, in helix A9 and the following loop (Fig. 8*A*). In particular helix A9, which is a 3_{10} helix in the protein, is reorganized as a regular α-helix in the PmaLAAD-01N/anthranilate complex. Notably, this region is part of the PmaLAAD-01N-specific α+β subdomain and is located at the entrance of the substrate-binding pocket.

Such an entrance is unusually wide (15-20 Å, calculated from the Cα position of residues located on opposite sides of the entrance) and mainly negatively charged (Glu109, Asp145, Asp150, Glu154, Glu341, Asp417, Glu418) (Fig. 8*F*). The substrate-binding pocket is deep (≈ 20 Å) and mostly hydrophobic; the anthranilate aromatic ring is stacked to the FAD isoalloxazine ring, at a distance of ≈ 4 Å, and located in a pocket lined by Leu279, Phe318, Val412, Val438 and Trp439. The ligand carboxyl group is H-bonded to the NE and NH_2 atoms of Arg316 side chain (2.8 Å and 3.2 Å, respectively), to the NE2 atom of Gln100 side chain (2.9 Å), and to the FAD O4 atom (3.3 Å), while the 2-amino group of the ligand is H-bonded to the carbonyl oxygen of Val438 (3.2 Å). Upon ligand binding, Arg316 changes its conformation dramatically and inserts its side chain into the active site and forms an H-bond, together with Gln100, with anthranilate at the *re* side of the isoalloxazine ring (Fig. 8*A*,*B*). Additionally, the Phe318 also changes rotamer, orienting its side chain parallel to the ligand aromatic ring, at a distance of ≈ 5 Å, and the structural changes occurring in the 316-318 region are transmitted to the adjacent 333-343 region, which is located at the entrance of the substrate-binding pocket (Fig. 8*A*,*B*).

The PmaLAAD-01N/anthranilate complex is well suited to analyse the binding mode of L-Phe (Fig. 8*C*). The PmaLAAD-01N enzymatic activity recorded on the synthetic amino acid L-Phe ethylester (33% in comparison with L-Phe) finds its structural explanation in the presence of a pocket lined by Tyr98, Ala314 and Arg316, where the ethylester moiety of the substrate fits nicely (Fig. 8*D*). In contrast, binding of the D-isomer of Phe would instead result in a steric clash between its aromatic side chain and the FAD isoalloxazine moiety (Fig. 8*E*), in keeping with the absence of activity assayed for D-amino acids.

DISCUSSION

PmaLAAD is a FAD-containing enzyme which catalyzes the stereoselective deamination of L-amino acids into the corresponding α-keto acids and ammonia without forming hydrogen peroxide, thus differing from known LAAOs. PmaLAAD shows a broad substrate specificity with a preference for neutral, aromatic L-amino acids: the highest activity is apparent for L-Phe, L-Leu, L-Met and L-Trp (Table 2). This agrees with the size and microenvironment of the substrate-binding pocket, which is lined by hydrophobic residues (Fig. 8*B*).

PmaLAAD is a membrane-bound enzyme. Subcellular fractionation and deletion of N-terminus segments demonstrated that PmaLAAD is anchored to the membrane through a putative transmembrane α-helix (residues 8-28). The cellular localization is fundamental for enzyme function: accordingly, we demonstrated that PmaLAAD is fully active in the presence of membranes only. The purified full-length, membrane-devoid, PmaLAAD-00N variant is practically inactive and the catalytic competence is acquired by adding exogenous crude *E. coli* membranes, but is only marginally increased using synthetic membranes produced from highly pure *E. coli* lipid extracts (Table 3). These results indicate that PmaLAAD requires a specific membrane partner for its activity, rather than a generic hydrophobic environment of the membrane. From spectral evidence (Fig. 4*B*), and because cytochrome c is not considered to be part of the main electron transport chain in the *Proteus* genus (37), we propose that the physiological electron acceptor from PmaLAAD could be a b-type cytochrome, a membrane protein that accepts electrons from different donors.

We demonstrated that the appearance of an absorbance spectrum likely corresponding to reduced cytochrome b is observed only under anaerobic conditions, while under aerobiosis electrons are transferred to dioxygen by the respiratory chain, as observed using the polarographic assay. Indeed, PmaLAAD-00N re-oxidized very slowly on dioxygen, while in DAAOs and LAAOs $FADH_2$ reacted quickly with O_2 (4,35,47): in PmaLAAD the rate constant for $FADH_2$ re-oxidation by O_2 is ≈ 100-fold slower than the turnover number. This limited direct O_2 re-oxidation of $FADH_2$ explains the inability of PmaLAAD to produce hydrogen peroxide and classifies this enzyme outside the oxidase class of flavoenzymes (33), whose members represent the closest structural relatives (Fig. 5*C* and Fig. 6).

It should be noted that reactivity of flavoproteins toward dioxygen is related to the microenvironment of their isoalloxazine ring, in particular to the presence of positively charged residues in proximity of the FAD C4a position. For instance, in LAAO from snake venom, Lys326 is present on the *si* face of FAD, and in glucose oxidases two His residues are located on the *re* face of the cofactor (48,49). In contrast, in PmaLAAD, the corresponding positions in the vicinity of the isoalloxazine moiety of FAD are occupied by the neutral Gln281 and the hydrophobic residues Trp439 and Val438. Nevertheless, the isoalloxazine ring is exposed to solvent in PmaLAAD, especially at the N5 site and its location is compatible with electron transfer to a bound acceptor protein.

The FAD cofactor is bound in an extended conformation (Fig. 7*A*) and establishes a high number of interactions with PmaLAAD apoprotein, comprising the interaction of helix dipole A14 with the O2 of the isoalloxazine ring that is expected to stabilize the anionic form of $FADH_2$. The isoalloxazine ring is located at the interface between the substrate and the FAD-binding domains and is exposed to solvent, especially at the N5 site: its location is compatible with electron transfer to the bound acceptor protein.

The overall fold of PmaLAAD resembles that of known amine or amino acid oxidases/dehydrogenases (Fig. 6) but with specific structural features that allow it to fulfil a different role, *i.e.* the deamination of L-amino acid with no hydrogen peroxide production to fuel the membrane electron-transfer (respiratory) chain. Indeed, phylogenetic analysis demonstrates that proteins highly homologous to PmaLAAD (≥ 28% sequence identity) are present only in the Proteobacteria phylum, and in particular in the subphyla of alpha-, beta- and gamma-proteobacteria (Fig. 9). Worthy of note is that all related sequences belong to putative flavoprotein oxidases or deaminases with unknown function, while the sequence identity with known microbial DAAOs or LAAOs is quite low (*i.e.* between 13.9% and 16.4%). This finding suggests that LAADs diverged early from amino acid oxidases but conserved a similar active-site organization related to the use of the same substrate. In common with known amino acid oxidases, PmaLAAD shows not only the fold but also the ability to generate the anionic semiquinone form of FAD during photoreduction, and to produce charge-transfer complexes following binding of carboxylic acids.

Different from other flavooxidases, PmaLAAD possesses an additional α+β subdomain that is placed in a key (structural and functional) region of the protein. As a matter of fact, the putative transmembrane α-helix of PmaLAAD is bound to the N-terminal end of this domain (residues 29-56) while its C-terminal end encompasses the region of the active-site entrance (helix A9 and following loop) that changes conformation upon ligand binding (Fig. 8A). Indeed, comparison of the free and anthranilate-bound structures of PmaLAAD-01N shows that part of the active site, in particular Arg316 (which binds the carboxyl group of substrate) and Phe318 (which forms hydrophobic interactions with the apolar moiety of the ligand), only acquires the correct geometry in the presence of the substrate (Fig. 8*A*). We propose that these conformational changes could favour the binding (by electrostatic interactions) and correct orientation of the substrate at the active site of the enzyme. This behaviour is not observed in canonical flavoprotein oxidases such as DAAOs or LAAOs (4,47,50).

In summary, we solved the first three-dimensional structure of a L-amino acid deaminase and set up a procedure to prepare a stable and soluble preparation of the PmaLAAD form (containing membrane fragments) that can be employed in cell-free biocatalysis. Overall, these results provide the basis for pushing protein engineering studies aimed to manipulate LAAD substrate specificity in order to fulfil different biotechnological requests, such as the resolution of racemic mixtures of natural and unnatural amino acids or the generation of novel, synthetic biochemical pathways (1,51).

Acknowledgements: The gene encoding for LAAD from *P. myxofaciens* was a generous gift of Wolfgang Kroutil (University of Graz). We thank prof. Martino Bolognesi for helpful discussion.

Conflict of interest: The authors declare that they have no conflicts of interest with the content of this article.

Author contributions: PM and GM performed biochemical experiments, analysed the experimental data and wrote the manuscript. MN performed the crystallization trials, solved the structure and wrote the manuscript. LP designed experiments, analysed the data and wrote the manuscript.

REFERENCES

1. Turner, N. J. (2004) Enzyme catalysed deracemisation and dynamic kinetic resolution reactions. *Curr. Opin. Chem. Biol.* **8**, 114-119
2. Pollegioni, L., and Molla, G. (2011) New biotech applications from evolved D-amino acid oxidases. *Trends Biotechnol.* **29**, 276-283
3. Pollegioni, L., Sacchi, S., Caldinelli, L., Boselli, A., Pilone, M.S., Piubelli, L., and Molla, G. (2007) Engineering the properties of D-amino acid oxidases by a rational and a directed evolution approach. *Curr. Protein Pept. Sci.* **8**, 600-618
4. Pollegioni, L., Motta, P., and Molla, G. (2013) L-amino acid oxidase as biocatalyst: a dream too far? *Appl. Microbiol. Biotechnol.* **97**, 9323-9341
5. Pantaleone, D. P., Geller, A. M., and Taylor, P. P. (2001) Purification and characterization of an L-amino acid deaminase used to prepare unnatural amino acids. *J. Mol. Catal. B: Enzym.* **11**, 795-803
6. Busto, E., Richter, N., Grischek, B., and Kroutil, W. (2014) Biocontrolled formal inversion or retention of L-α-amino acids to enantiopure (R)- or (S)-hydroxyacids. *Chemistry* **20**, 11225-11228
7. Hou, Y., Hossain, G. S., Li, J., Shin, H. D., Liu, L., and Du, G. (2015) Production of phenylpyruvic acid from L-phenylalanine using an L-amino acid deaminase from *Proteus mirabilis*: comparison of enzymatic and whole-cell biotransformation approaches. *Appl. Microbiol. Biotechnol.* **99**, 8391-8402
8. Giammanco, G. M., Grimont, P. A., Grimont, F., Lefevre, M., Giammanco, G., and Pignato, S. (2011) Phylogenetic analysis of the genera *Proteus*, *Morganella* and *Providencia* by comparison of *rpoB* gene sequences of type and clinical strains suggests the reclassification of *Proteus myxofaciens* in a new genus, *Cosenzaea* gen. nov., as *Cosenzaea myxofaciens* comb. nov. *Int. J. Syst. Evol. Microbiol.* **61**, 1638-1644
9. Caldinelli, L., Sacchi, S., Molla, G., Nardini, M., and Pollegioni, L. (2013) Characterization of human DAAO variants potentially related to an increased risk of schizophrenia. *Biochim. Biophys. Acta* **1832**, 400-410
10. Volontè, F., Marinelli, F., Gastaldo, L., Sacchi, S., Pilone, M. S., Pollegioni, L., and Molla, G. (2008) Optimization of glutaryl-7-aminocephalosporanic acid acylase expression in *E. coli*. *Protein Expr. Purif.* **61**, 131-137
11. Molla, G., Piubelli, L., Volontè, F., and Pilone, M. S. (2012) Enzymatic detection of D-amino acids. *Methods Mol. Biol.* **794**, 273-289
12. Harris, C. M., Pollegioni, L., and Ghisla, S. (2001) pH and kinetic isotope effects in D-amino acid oxidase catalysis. *Eur. J. Biochem.* **268**, 5504-5520
13. Molla, G., Porrini, D., Job, V., Motteran, L., Vegezzi, C., Campaner, S., Pilone, M. S., and Pollegioni, L. (2000) Role of arginine 285 in the active site of *Rhodotorula gracilis* D-amino acid oxidase. A site-directed mutagenesis study. *J. Biol. Chem.* **275**, 24715-24721
14. Harris, C. M., Molla, G., Pilone, M. S., and Pollegioni, L. (1999) Studies on the reaction mechanism of *Rhodotorula gracilis* D-amino-acid oxidase. Role of the highly conserved Tyr-223 on substrate binding and catalysis. *J. Biol. Chem.* **274**, 36233-26240
15. Caldinelli, L., Iametti, S., Barbiroli, A., Bonomi, F., Fessas, D., Molla, G., Pilone, M. S., and Pollegioni, L. (2005) Dissecting the structural determinants of the stability of cholesterol oxidase containing covalently bound flavin. *J. Biol. Chem.* **280**, 22572-22581

16. Kabsch, W. (2010) XDS. *Acta Crystallogr. D Biol. Crystallogr.* **66**, 125-132
17. Evans, P. (2006) Scaling and assessment of data quality. *Acta Crystallogr. D Biol. Crystallogr.* **62**, 72-82
18. Storoni, L. C., McCoy, A. J., and Read, R. J. (2004) Likelihood-enhanced fast rotation functions. *Acta Crystallogr. D Biol. Crystallogr.* **60**, 432-438
19. Chen, Z. W., Hassan-Abdulah, A., Zhao, G., Jorns, M. S., and Mathews, F. S. (2006) Heterotetrameric sarcosine oxidase: structure of a diflavin metalloenzyme at 1.85 Å resolution. *J. Mol. Biol.* **360**, 1000-1018
20. Adams, P. D., Afonine, P. V., Bunkóczi, G., Chen, V. B., Davis, I. W., Echols, N., Headd, J. J., Hung, L. W., Kapral, G. J., Grosse-Kunstleve, R. W., McCoy, A. J., Moriarty, N. W., Oeffner, R., Read, R. J., Richardson, D. C., Richardson, J. S., Terwilliger, T. C., and Zwart, P. H. (2010) PHENIX: a comprehensive Python-based system for macromolecular structure solution. *Acta Crystallogr. D Biol. Crystallogr.* **66**, 213-221
21. Emsley, P., and Cowtan, K. (2004) Coot: model-building tools for molecular graphics. *Acta Crystallogr. D Biol. Crystallogr.* **60**, 2126-2132
22. Murshudov, G. N., Vagin, A. A., and Dodson, E. J. (1997) Refinement of macromolecular structures by the maximum-likelihood method. *Acta Crystallogr. D Biol. Crystallogr.* **53**, 240-255
23. Chen, V. B., Arendall 3rd, W. B., Headd, J. J., Keedy, D. A., Immormino, R. M., Kapral, G. J., Murray, L. W., Richardson, J. S., and Richardson, D. C. (2010) MolProbity: all-atom structure validation for macromolecular crystallography. *Acta Crystallogr. D Biol. Crystallogr.* **66**, 12-21
24. Finn, R. D., Clements, J., and Eddy, S. R. (2011) HMMER web server: interactive sequence similarity searching. *Nucleic Acids Res*. **39**, W29-W37
25. Chen, C., Natale, D. A., Finn, R.D., Huang, H., Zhang, J., Wu, C.H., and Mazumder, R. (2011) Representative proteomes: a stable, scalable and unbiased proteome set for sequence analysis and functional annotation. *PLoS One* **6**, e18910
26. Huang, Y., Niu, B., Gao, Y., Fu, L., and Li, W. (2010) CD-HIT Suite: a web server for clustering and comparing biological sequences. *Bioinformatics* **26**, 680-682
27. Gouy, M., Guindon, S., and Gascuel, O. (2010) SeaView version 4: A multiplatform graphical user interface for sequence alignment and phylogenetic tree building. *Mol. Biol. Evol*. **27**, 221-224
28. Guindon, S., Dufayard, J. F., Lefort, V., Anisimova, M., Hordijk, W., and Gascuel, O. (2010) New algorithms and methods to estimate maximum-likelihood phylogenies: assessing the performance of PhyML 3.0. *Syst. Biol*. 59, 307-321
29. Felsenstein, J. (1985) Confidence limits on phylogenies: an approach using the bootstrap. *Evolution* **39**, 783-791
30. Baek, J. O., Seo, J. W., Kwon, O., Seong, S. I., Kim, I. H., and Kim, C. H. (2011) Expression and characterization of a second L-amino acid deaminase isolated from *Proteus mirabilis* in *Escherichia coli*. *J. Basic Microbiol.* **51**, 129-135
31. Fonda, M. L., and Anderson, B. M. (1968) D-amino acid oxidase. II. Studies of substrate-competitive inhibitors. *J. Biol. Chem.* **243**, 1931-1935
32. Sacchi, S., Caldinelli, L., Cappelletti, P., Pollegioni, L., and Molla, G. (2012) Structure-function relationships in human D-amino acid oxidase. *Amino Acids* **43**, 1833-1850
33. Massey, V., and Hemmerich, P. (1980) Active-site probes of flavoproteins. *Biochem. Soc. Trans.* **8**, 246-257
34. Pawelek, P. D., Cheah, J., Coulombe, R., Macheroux, P., Ghisla, S., and Vrielink, A. (2000) The structure of L-amino acid oxidase reveals the substrate trajectory into an enantiomerically conserved active site. *EMBO J.* **19**, 4204-4215
35. Pollegioni, L., Langkau, B., Tischer, W., Ghisla, S., and Pilone, M. S. (1993) Kinetic mechanism of D-amino acid oxidases from *Rhodotorula gracilis* and *Trigonopsis variabilis*. *J. Biol. Chem.* **268**, 13850-13857
36. Volbeda, A., Darnault, C., Parkin, A., Sargent, F., Armstrong, F. A., and Fontecilla-Camps, J. C. (2012) Crystal structure of the O-tolerant membrane-bound hydrogenase 1 from *Escherichia coli* in complex with its cognate cytochrome b. *Structure* **21**, 184-190
37. van Wielink, J. E., Reijnders, W. N., Oltmann, L. F., and Stouthamer, A. H. (1983) Electron transport and cytochromes in aerobically grown *Proteus mirabilis*. *Arch. Microbiol.* **136**, 152-157
38. van Wielink, J. E., Reijnders, W. N., Oltmann, L. F., Leeuwerik, F. J., and Stouthamer, A. H. (1983) The membrane-bound b and c-type cytochromes of *Proteus mirabilis* grown under different

conditions. Characterization by means of coupled spectrum deconvolution and potentiometric analysis. *Arch Microbiol.* **134**,118-122
39. Shabbiri K, Ahmad W, Syed Q, Adnan A. (2010) Isolation and purification of complex II from *Proteus Mirabilis* strain ATCC 29245. *Braz. J. Microbiol.* **41**,796-804
40. Hofmann, K., and Stoffel, W. (1993) TMbase - A database of membrane spanning proteins segments. *Biol. Chem. Hoppe-Seyler* **374**,166
41. Dym, O., and Eisenberg, D. (2001) Sequence-structure analysis of FAD-containing proteins. *Protein Sci.* **10**, 1712-1728
42. Holm, L., and Rosenström, P. (2010) Dali server: conservation mapping in 3D. *Nucl. Acids Res.* **38**, W545-W549
43. Krissinel, E., and Henrick, K. (2007) Inference of macromolecular assemblies from crystalline state. *J. Mol. Biol.* **372**, 774-797
44. Tsuge, H., Kawakami, R., Sakuraba, H., Ago, H., Miyano, M., Aki, K., Katunuma, N., and Ohshima, T. (2005) Crystal structure of a novel FAD-, FMN-, and ATP-containing L-proline dehydrogenase complex from *Pyrococcus horikoshii*. *J. Biol. Chem.* **280**, 31045-31049
45. Mörtl, M., Diederichs, K., Welte, W., Molla, G., Motteran, L., Andriolo, G., Pilone, M. S., and Pollegioni, L. (2004) Structure-function correlation in glycine oxidase from *Bacillus subtilis*. *J. Biol. Chem.* **279**, 29718-29727
46. Moriguchi, T., Ida, K., Hikima, T., Ueno, G., Yamamoto, M., and Suzuki, H. (2010) Channeling and conformational changes in the heterotetrameric sarcosine oxidase from *Corynebacterium* sp. U-96. *J. Biochem.* **148**, 491-505
47. Pawelek, P. D., Cheah, J., Coulombe, R., Macheroux, P., Ghisla, S., and Vrielink, A. (2000) The structure of L-amino acid oxidase reveals the substrate trajectory into an enantiomerically conserved active site. *EMBO J.* **19**, 4204-4215
48. Mattevi, A. (2006) To be or not to be an oxidase: challenging the oxygen reactivity of flavoenzymes. *Trends Biochem. Sci.* **31**, 276-283
49. Saam, J., Rosini, E., Molla, G., Schulten, K., Pollegioni, L., and Ghisla, S. (2010) O_2 reactivity of flavoproteins: dynamic access of dioxygen to the active site and role of a H^+ relay system in D-amino acid oxidase. *J. Biol. Chem.* **285**, 24439-24446
50. Umhau, S., Pollegioni, L., Molla, G., Diederichs, K., Welte, W., Pilone, M. S., and Ghisla, S. (2000) The X-ray structure of D-amino acid oxidase at very high resolution identifies the chemical mechanism of flavin-dependent substrate dehydrogenation. *Proc. Natl. Acad. Sci. USA* **97**, 12463-12468
51. Tessaro, D., Pollegioni, L., Piubelli, L., D'Arrigo, P., and Servi, S. (2015) Systems biocatalysis: an artificial metabolism for interconversion of functional groups. *ACS Catal.* **5**, 1604-1608
52. Collaborative Computational Project Number 4 (1994) The CCP4 Suite: Programs for Protein Crystallography. *Acta Crystallogr. D Biol. Crystallogr.* **50**, 760-76348.

FOOTNOTES

This work was supported by a grant from Fondo di Ateneo per la Ricerca to GM and LP. PM is a PhD student of the Degree in Analysis, Protection and Management of Biodiversity at the Università degli Studi dell'Insubria.

The abbreviations used are: AT, aminotransferase; DAAO, D-amino acid oxidase; Fbd, FAD binding domain; MPD, 2-Methyl-2,4-pentanediol; LAAD, L-amino acid deaminase; LAAO, L-amino acid oxidases; PmaLAAD, L-amino acid deaminase from *Proteus myxofaciens*; PmaLAAD-00C, C-terminal His-tagged PmaLAAD; PmaLAAD-00N, N-terminal His-tagged PmaLAAD; PmaLAAD-01N, truncated PmaLAAD-00N starting from Met28; PmaLAAD-02N, truncated PmaLAAD-00N starting from Ala50; Sbd, substrate binding domain.

FIGURE LEGENDS

FIGURE 1. **Amino acid sequence of PmaLAAD variants produced in this work.** *A*, scheme of produced PmaLAAD variants showing the putative transmembrane α-helix. *B*, sequence comparison of produced PmaLAAD variants; residues are numbered as in PmaLAAD wild-type. Black and grey boxes: HisTag and GXGXXG sequences, respectively. PmaLAAD-00N and PmaLAAD-00C possess an additional sequence (made of nine and eight residues, respectively) as compared to the wild-type enzyme.

FIGURE 2. **Purification scheme of recombinant PmaLAAD variants from *E. coli* cells.** *A,* purification scheme of recombinant wild-type PmaLAAD *(left)*, PmaLAAD-00N *(centre)* and PmaLAAD-01N *(right)*. Boxed numbers refer to lanes in the corresponding SDS–PAGE panel *B*. Gels were stained with Coomassie blue; (M) prestained protein ladder. Loaded samples corresponds to 100 µL of cell culture for PmaLAAD (*lef*t) and PmaLAAD-01N (*right*) and to 50 µL for PmaLAAD-00N (*centre*). S.A. = LAAD specific activity on L-Phe; I.B. = inclusion bodies; F.T. = flow through.

FIGURE 3. **Apparent kinetic parameters on L-Phe and pH and temperature dependence of the activity of PmaLAAD.** *A*, enzymatic activity of PmaLAAD on the crude extract was determined at air saturation by the increase of the product phenylpyruvate, pH 7.5 and 25 °C. Data points were fitted with a Michaelis-Menten equation. *B*, activity of PmaLAAD at 25 °C at the indicated pH values in multicomponent buffer (12). Data are expressed as percentage of maximal enzyme activity and were fitted based on the equation for two dissociations (12); estimated pK_{a1} was 5.8 ± 0.1 and pK_{a2} was 8.3 ± 0.3. *C*, activity of PmaLAAD determined at the indicated temperatures. Data are expressed as percentage of enzyme activity assayed at 50 °C (the maximum value). In panels *B* and *C*, activity was determined on 25 mM L-Phe (and at pH 7.5 in panel C) employing 10 µL (corresponding to 25 µg of enzyme) of resuspended membrane containing PmaLAAD fraction. Bars indicate ± SE for three determinations.

FIGURE 4. **Spectral properties of PmaLAAD-00N and PmaLAAD-01N variants.** *A,* absorbance spectrum of PmaLAAD-00N in the oxidized and reduced form, obtained by anaerobic addition of 25 mM L-Phe (full line), and of PmaLAAD-01N (dashed line) in the oxidized form. *B*, absorbance spectrum of 17 µM PmaLAAD-00N in the oxidized and reduced form (dotted line) by anaerobic addition of 25 mM L-Phe in the presence of *E. coli* membranes. Dashed line represents the spectral species obtained after the first (faster and wider) reduction phase (see main text). *C*, *D*, binding of anthranilate to 15 µM PmaLAAD-00N and 14.6 µM PmaLAAD-01N, respectively. Selected spectra obtained upon addition of increasing concentrations of anthranilate are shown. *E,* binding of kojic acid to 15 µM PmaLAAD-00N; selected spectra obtained upon addition of increasing ligand concentrations (up to 242 mM) are shown. *F,* binding of 2-aminobenzaldehyde (up to 10 mM) to PmaLAAD-01N variant. *G,* spectra recorded at different times during photoreduction of 20 µM PmaLAAD-00N; the maximal amount of reduced flavin species (dashed line) was detected after 5 min of photoillumination. The photoreduced enzyme was anaerobically mixed with benzyl viologen yielding the re-oxidized enzyme after 45 min of incubation (dotted line). *H,* spectra recorded at different times during photoreduction of 17 µM PmaLAAD-00N in the presence of *E. coli* membranes (from 280 mg of cells); the maximal amount of reduced flavin species (dashed line) was detected after 3.5 min of photoillumination. Bold line: spectrum of the original, oxidized enzyme. The arrows in panels indicate the direction of absorbance change at increasing ligand concentrations (panels *C*-*F*) or at different times (panels *G* and *H*). All insets: the observed increase in absorbance at selected wavelengths is plotted as a function of the ligand concentration: the solid line is a fit of the data to a hyperbolic binding curve. Spectra were recorded in 50 mM potassium phosphate, pH 7.5 and 15 °C. K_d values reported in the text are the average ± SE of 3 determinations.

FIGURE 5. **Crystal structure of PmaLAAD-01N, topology and structure-based sequence alignment.** *A*, schematic view of the domain spatial arrangement in PmaLAAD-01N. The FAD binding domain is in green (with the α+β additional subdomain in blue), the substrate binding domain in orange; α-helices, β -strands, and coils are represented by helical ribbons, arrows, and ropes, respectively. The FAD cofactor is shown in stick representation (yellow color). The N- and C-termini of PmaLAAD-01N are labelled. *B*, secondary structure topology diagram of PmaLAAD-01N: cylinders and arrows indicate

helices and strands, respectively. *C*, structure-based sequence alignment of PmaLAAD-01N. PmaLAAD-01N is aligned with L-proline dehydrogenase from *Pyrococcus horikoshii* (PDB code 1Y56), glycine oxidase from *Bacillus subtilis* (PDB code 1C0I) and heterotetrameric sarcosine oxidases from *Corynebacterium* sp. U-96 (PDB code 3ADA) and from *Stenotrophomonas maltophilia* (PDB code 2GAG). The sequence alignment has been performed using the CLUSTALW program (http://www.ebi.ac.uk/Tools/msa/clustalw2/) and manually corrected based on their three-dimensional structure comparisons. PmaLAAD-01N secondary structure elements are shown on the top of the alignment and shaded in gray (yellow for 3_{10} helices) for all aligned proteins. Asterisks and circles indicate PmaLAAD-01N residues interacting with the FAD isoalloxazine ring and with anthranilate, respectively.

FIGURE 6. **Structural comparison with related proteins.** *A*, the structural comparison is produced by superimposing the FAD binding domains of PmaLAAD-01N (green, α+β subdomain blue) with L-proline dehydrogenase from *Pyrococcus horikoshii* (PDB code 1Y56, orange), or glycine oxidase from *Bacillus subtilis* (PDB code 1C0I, magenta), or heterotetrameric sarcosine oxidase from *Corynebacterium sp.* U-96 (PDB code 3ADA, cyan) and from *Stenotrophomonas maltophilia* (PDB code 2GAG, yellow). The FAD cofactor bound to the PmaLAAD-01N is shown in stick representation (green color). *B*, the different orientation of the N-terminus in PmaLAAD-01N relative to the heterotetrameric sarcosine oxidase from *Corynebacterium sp.* U-96 (PDB code 3ADA, cyan) and from *Stenotrophomonas maltophilia* (PDB code 2GAG, yellow) is shown. PmaLAAD-01N Leu52 is labelled to indicate the position where the backbone of the three proteins starts to show a good superimposition. In both panels the FAD cofactor bound to the PmaLAAD-01N FAD-binding domain is shown in stick representation (green color).

FIGURE 7. **FAD structure, protein–isoalloxazine ring interactions and active site cavity of PmaLAAD-01N.** *A,* simulated annealing (|Fo| - |Fc|) omit electron density map (contoured at 3σ, grey mesh) for the FAD cofactor. The absolute values of the electron density map are reported in the figure inset, as calculated by the FFT program implemented in the CCP4i software package (52). The map refers to the high resolution data at 1.75 Å, but a similar result can be obtained also from the 2.0 Å resolution data (see Table 1). *B,* the FAD molecule (yellow) and the protein residues (green) located at the active site cavity relevant for FAD binding are shown in stick representation and labeled. A water molecule is represented as red sphere (0.3 vdW radius). H-bonds are shown by dashed lines. *C,* model of the N5-sulfo-FAD molecule bound to PmaLAAD-01N based on the isoalloxazine ring of a N5-sulfo-flavin mononucleotide molecule (PDB code 1QCW).

FIGURE 8. **Ligand binding to PmaLAAD-01N.** *A,* structural reorganization of the substrate binding pocket in PmaLAAD subunit B upon anthranilate binding. The bound anthranilate (ANT) is shown in stick representation (cyan) surrounded by its 2Fo-Fc electron density, contoured at 1σ (cyan mesh). The structure of the PmaLAAD-01N/anthranilate complex (color code as in Figure 5) is superimposed to the unbound PmaLAAD-01N (grey) to highligth the backbone differences in the regions 316-318 (the β18-β19 loop) and 333-343 (helix A9 and the following loop), and the side-chain structural variations of Arg316 and Phe318. *B,* substrate binding pocket in PmaLAAD-01N. The bound anthranilate, the FAD molecule and the relevant protein residues are shown in stick representation and labelled. Dashed lines indicate H-bonds. For clarity, the A9 region shown in panel A has been omitted. Modeling of the bound *C,* L-Phe, *D,* L-Phe ethylester, and *E,* D-Phe, based on the PmaLAAD-01N/anthranilate complex. *F,* entrance of the active site. Molecular surface of PmaLAAD-01N, colored according to its potential (blue positive, red negative). The entry of the active site cavity, showing the isoalloxazine ring of FAD (yellow) and the bound anthranilate (grey), is clearly visible.

FIGURE 9. **Phylogenetic analysis.** Proteins homologous to PmaLAAD (> 28% sequence identity) are only present in the *Proteobacteria* phylum, in particular in the subphyla of alphaproteobacteria, betaproteobacteria and gammaproteobacteria. Homologous proteins form three main clusters and an isolated sequence (B): a group close to PmaLAAD (LAAD) and two large groups (A and C). Noteworthy, all identified proteins are putative flavoprotein oxidases or deaminases with unknown function. Numbers on the branches represent the percentage of bootstrap samples supporting the branch (only values > 50% are shown). PmaLAAD is indicated by an arrow. Sequences were identified by their

UniProtKB Accession Number.

FIGURES AND TABLES

TABLE 1
Data collection and refinement statistics

Numbers given in parentheses are from the last resolution shell.

Data Collection	**PmaLAAD-01N**	**PmaLAAD-01N + anthranilate**
X-Ray source	ESRF ID23-2	ESRF ID23-1
Space group	$P2_1$	$P2_1$
Unit cell dimensions:		
a, b, c (Å)	72.76, 93.71, 74.69	72.81, 93.32, 75.07
α, β, γ (°)	90, 102.85, 90	90, 103.22, 90
Resolution (Å)	49.08-2.00 (2.11-2.00)	45.90-1.75 (1.84-1.75)
Observations	298242	257980
Unique reflections	65982	96409
R-merge (%)[a]	9.4 (51.4)	3.4 (51.3)
I/σ(I)	12.0 (2.9)	14.9 (1.9)
Completeness (%)	99.9 (99.9)	98.1 (97.9)
Multiplicity	4.5 (4.7)	2.7 (2.7)
Refinement		
R-factor/R-free (%)[b]	17.7/20.9	15.6/19.7
Protein residues in the a.u.	2x447 (28-474)	2x447 (28-474)
FAD	2	2
Anthranilic acid	-	2
Water molecules	518	546
Model quality		
Average B-factor (Å^2):		
Protein	26.0	36.8
FAD	16.2	22.9
ligand	-	41.8
water	31.7	43.4
Rmsd from ideal values:		
bond lengths (Å)	0.006	0.005
bond angles (°)	1.137	1.098
Ramachandran plot:		
most favored regions	96.8	96.6
additional allowed regions	3.2	3.4

[a] $R_{merge} = \Sigma_h\Sigma_i \mid I_{hi} - \langle I_h \rangle \mid / \Sigma_h\Sigma_i I_{hi}$

[b] $R_{factor} = \Sigma_h \mid\mid F_{obs}\mid - \mid F_{calc}\mid\mid / \Sigma_h \mid F_{obs}\mid$, with F_{obs} being the observed and F_{calc} the calculated structure factor amplitudes

TABLE 2
Relative specific activity of PmaLAAD on different substrates

The activity was determined by the polarographic assay (oxygen consumption) using a membrane-containing PmaLAAD preparation and 25 mM substrate concentration with the exception of L-Tyr (1.25 mM), β^3-Phe (12.5 mM), 1-naphthyl-Ala (0.375 mM) and Gly (0.375 mM). The reported value was the average of three determinations. *Specific activity was expressed as percentage of the value assessed with L-Phe (100%). **The activity value for the corresponding D-amino acid was ≤ 4%. ***The activity on this compound was confirmed by using for the assay a purified (by re-crystallization) substrate batch to avoid contamination by residual free L-Phe.

Amino acid	Specific activity (%)*	Amino acid	Specific activity (%)*,**
Neutral:		**Charged:**	
Gly	0.06	L-Asp	0.13
L-Ala	0.59	L-Glu	0.11
L-Pro	0.96	L-His	9.88
L-Ile	26.2	L-Lys	3.45
L-Val	3.47	L-Arg	8.0
L-Leu	99.2**	**Unnatural:**	
L-Met	86.0**	β-Ala	0.21
Aromatic:		β^2-Phe	0.24
L-Phe	100**	β^3-Phe	0.06
L-Tyr	13.7	D,L-tert-Leu	9.9
L-Trp	60.5**	L-Phe amide	2.29
Polar:		L-Phe-O-ethyl ester***	33.0
L-Cys	43.0**	1-Naphtyl-Gly	0.58
L-Ser	0	1-Naphtyl-Ala	3.75
L-Thr	0.09	2-Amino octanoic acid	0
L-Asn	0.74	3-Phenyl-Ser	3.49
L-Gln	0.55	Glufosinate	0.54
		D,L-DOPA	56.9

TABLE 3
PmaLAAD-00N activity recovery with purified *E. coli* lipid extracts

The activity was determined by the polarographic assay (oxygen consumption) on 25 mM L-Phe as a substrate, using ≈ 150 μg of purified protein. All mixtures have been sonicated before the assay, until the solution appeared completely clear.

Sample	Activity (U/mL)	Increase (-fold)
PmaLAAD-00N (control)	0.25 ± 0.06	1.0
PmaLAAD-00N + membranes from 45 mg cells	7.74 ± 0.37	31.5
PmaLAAD-00N + 4.5 mg Total Lipid extract	0.98 ± 0.13	4.0
PmaLAAD-00N + 4.5 mg Polar Lipid extract	0.39 ± 0.11	1.6
PmaLAAD-00N + membranes from 22.5 mg cells	3.45 ± 0.25	14.0
PmaLAAD-00N + membranes from 22.5 mg cells + 2.25 mg Total Lipid extract	4.96 ± 0.42	20.2
PmaLAAD-00N + membranes from 22.5 mg cells + 2.25 mg Polar Lipid extract	3.97 ± 0.15	16.1

TABLE 4

Structural comparison of proteins homologous to PmaLAAD-01N

PDB	chain	Z score	r.m.s. deviation			ali	nres	Id (%)	Protein	Ref.
			all	FbD	SbD					
1Y56	B	42.3	2.0 (361)	1.2 (179)	2.0 (174)	361	374	23	L-proline dehydrogenase complex from *Pyrococcus horikoshii*	(44)
1C0I	B	41.2	2.0 (353)	1.3 (176)	2.2 (171)	353	364	21	glycine oxidase from *Bacillus subtilis*	(45)
3ADA	B	40.9	2.2 (368)	1.3 (177)	1.9 (175)	368	397	23	heterotetrameric sarcosine oxidase from *Corynebacterium* sp. U-96.	(46)
2GAG	B	40.2	2.2 (368)	1.3 (176)	1.9 (176)	368	403	23	heterotetrameric sarcosine oxidase from *Stenotrophomonas maltophilia*	(19)

Figure 1

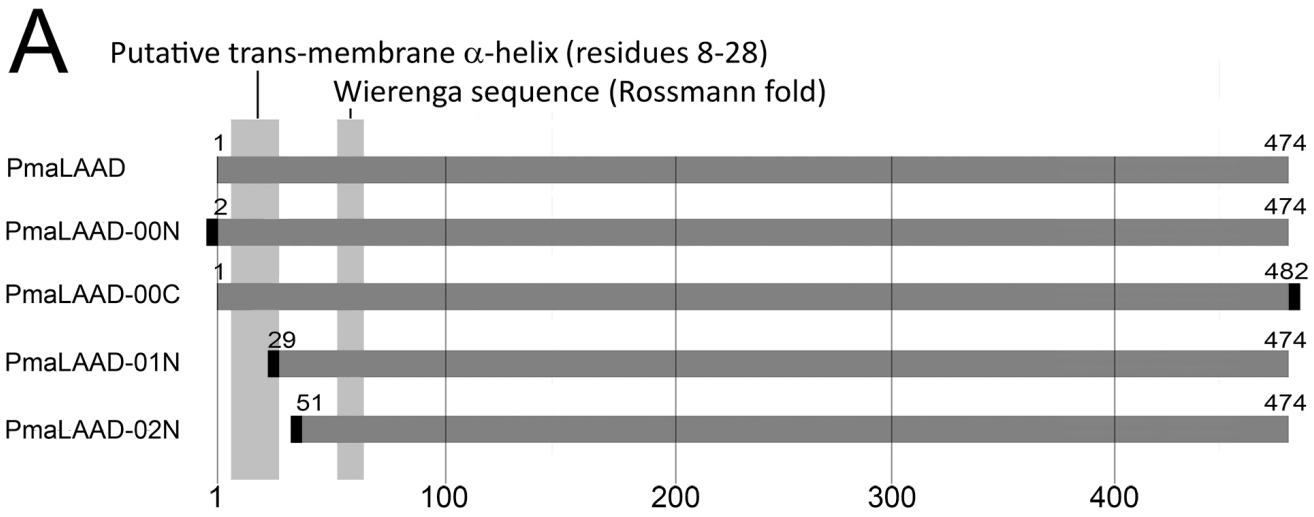

B

```
                                1       10        20        30        40        50        60        70        80
                                |       |         |         |         |         |         |         |         |
PmaLAAD                         MNISRRKLLLGVGAAGVLAGGAATLVPMVRRDGKFVESKSRALFVESTEGALPSESDVVIIGGGIQGIMTAINLAERGMS
PmaLAAD-00N                     MHHHHHHASNISRRKLLLGVGAAGVLAGGAATLVPMVRRDGKFVESKSRALFVESTEGALPSESDVVIIGGGIQGIMTAINLAERGMS
PmaLAAD-00C                     MNISRRKLLLGVGAAGVLAGGAATLVPMVRRDGKFVESKSRALFVESTEGALPSESDVVIIGGGIQGIMTAINLAERGMS
PmaLAAD-01N                                       MHHHHHHASMVRRDGKFVESKSRALFVESTEGALPSESDVVIIGGGIQGIMTAINLAERGMS
PmaLAAD-02N                                                       MHHHHHHASALPSESDVVIIGGGIQGIMTAINLAERGMS

                                90       100       110       120       130       140       150       160       170
                                |        |         |         |         |         |         |         |         |
PmaLAAD                         VTILEKGEVAGEQSGRAYSQIISYQTSPEIFPLHHYGKILWRGMNEKIGADTSYRTQGRVEALADEKALDRAQEWIKTAKETAGFDVPLN
PmaLAAD-00N                     VTILEKGEVAGEQSGRAYSQIISYQTSPEIFPLHHYGKILWRGMNEKIGADTSYRTQGRVEALADEKALDRAQEWIKTAKETAGFDVPLN
PmaLAAD-00C                     VTILEKGEVAGEQSGRAYSQIISYQTSPEIFPLHHYGKILWRGMNEKIGADTSYRTQGRVEALADEKALDRAQEWIKTAKETAGFDVPLN
PmaLAAD-01N                     VTILEKGEVAGEQSGRAYSQIISYQTSPEIFPLHHYGKILWRGMNEKIGADTSYRTQGRVEALADEKALDRAQEWIKTAKETAGFDVPLN
PmaLAAD-02N                     VTILEKGEVAGEQSGRAYSQIISYQTSPEIFPLHHYGKILWRGMNEKIGADTSYRTQGRVEALADEKALDRAQEWIKTAKETAGFDVPLN

                                180       190       200       210       220       230       240       250       260
                                |         |         |         |         |         |         |         |         |
PmaLAAD                         TRIIKGEELSNRLVGAQTPWTVAAFEEDSGSVDPETGTPTLARYAKQIGVKIYTHCAVRGIETAGGKISDVVTEKGAIRTSNVVLAGGIW
PmaLAAD-00N                     TRIIKGEELSNRLVGAQTPWTVAAFEEDSGSVDPETGTPTLARYAKQIGVKIYTHCAVRGIETAGGKISDVVTEKGAIRTSNVVLAGGIW
PmaLAAD-00C                     TRIIKGEELSNRLVGAQTPWTVAAFEEDSGSVDPETGTPTLARYAKQIGVKIYTHCAVRGIETAGGKISDVVTEKGAIRTSNVVLAGGIW
PmaLAAD-01N                     TRIIKGEELSNRLVGAQTPWTVAAFEEDSGSVDPETGTPTLARYAKQIGVKIYTHCAVRGIETAGGKISDVVTEKGAIRTSNVVLAGGIW
PmaLAAD-02N                     TRIIKGEELSNRLVGAQTPWTVAAFEEDSGSVDPETGTPTLARYAKQIGVKIYTHCAVRGIETAGGKISDVVTEKGAIRTSNVVLAGGIW

                                270       280       290       300       310       320       330       340       350
                                |         |         |         |         |         |         |         |         |
PmaLAAD                         SRLFMGNMGVDLPTLNVYLSQQRVSGVPGAPRGNVHLPNGIHFREQADGTYAVAPRIFTSSIVKDSFLLGPKFMHLLGGGELPLEFSIGE
PmaLAAD-00N                     SRLFMGNMGVDLPTLNVYLSQQRVSGVPGAPRGNVHLPNGIHFREQADGTYAVAPRIFTSSIVKDSFLLGPKFMHLLGGGELPLEFSIGE
PmaLAAD-00C                     SRLFMGNMGVDLPTLNVYLSQQRVSGVPGAPRGNVHLPNGIHFREQADGTYAVAPRIFTSSIVKDSFLLGPKFMHLLGGGELPLEFSIGE
PmaLAAD-01N                     SRLFMGNMGVDLPTLNVYLSQQRVSGVPGAPRGNVHLPNGIHFREQADGTYAVAPRIFTSSIVKDSFLLGPKFMHLLGGGELPLEFSIGE
PmaLAAD-02N                     SRLFMGNMGVDLPTLNVYLSQQRVSGVPGAPRGNVHLPNGIHFREQADGTYAVAPRIFTSSIVKDSFLLGPKFMHLLGGGELPLEFSIGE

                                360       370       380       390       400       410       420       430       440
                                |         |         |         |         |         |         |         |         |
PmaLAAD                         DLFNSFKMPTSWKLDEKSPFEQYRIATATQNTEHLDAVFQRMKTEFPVFEKSQIVERWGAVVSPTFDELPIISEVKEYPGLVINTATVWG
PmaLAAD-00N                     DLFNSFKMPTSWKLDEKSPFEQYRIATATQNTEHLDAVFQRMKTEFPVFEKSQIVERWGAVVSPTFDELPIISEVKEYPGLVINTATVWG
PmaLAAD-00C                     DLFNSFKMPTSWKLDEKSPFEQYRIATATQNTEHLDAVFQRMKTEFPVFEKSQIVERWGAVVSPTFDELPIISEVKEYPGLVINTATVWG
PmaLAAD-01N                     DLFNSFKMPTSWKLDEKSPFEQYRIATATQNTEHLDAVFQRMKTEFPVFEKSQIVERWGAVVSPTFDELPIISEVKEYPGLVINTATVWG
PmaLAAD-02N                     DLFNSFKMPTSWKLDEKSPFEQYRIATATQNTEHLDAVFQRMKTEFPVFEKSQIVERWGAVVSPTFDELPIISEVKEYPGLVINTATVWG

                                450       460       470       480
                                |         |         |         |
PmaLAAD                         MTEGPAAGEVTADIVTGKKPVIDPTPFSLDRFKK
PmaLAAD-00N                     MTEGPAAGEVTADIVTGKKPVIDPTPFSLDRFKK
PmaLAAD-00C                     MTEGPAAGEVTADIVTGKKPVIDPTPFSLDRFKKLEHHHHHH
PmaLAAD-01N                     MTEGPAAGEVTADIVTGKKPVIDPTPFSLDRFKK
PmaLAAD-02N                     MTEGPAAGEVTADIVTGKKPVIDPTPFSLDRFKK
```

Figure 2

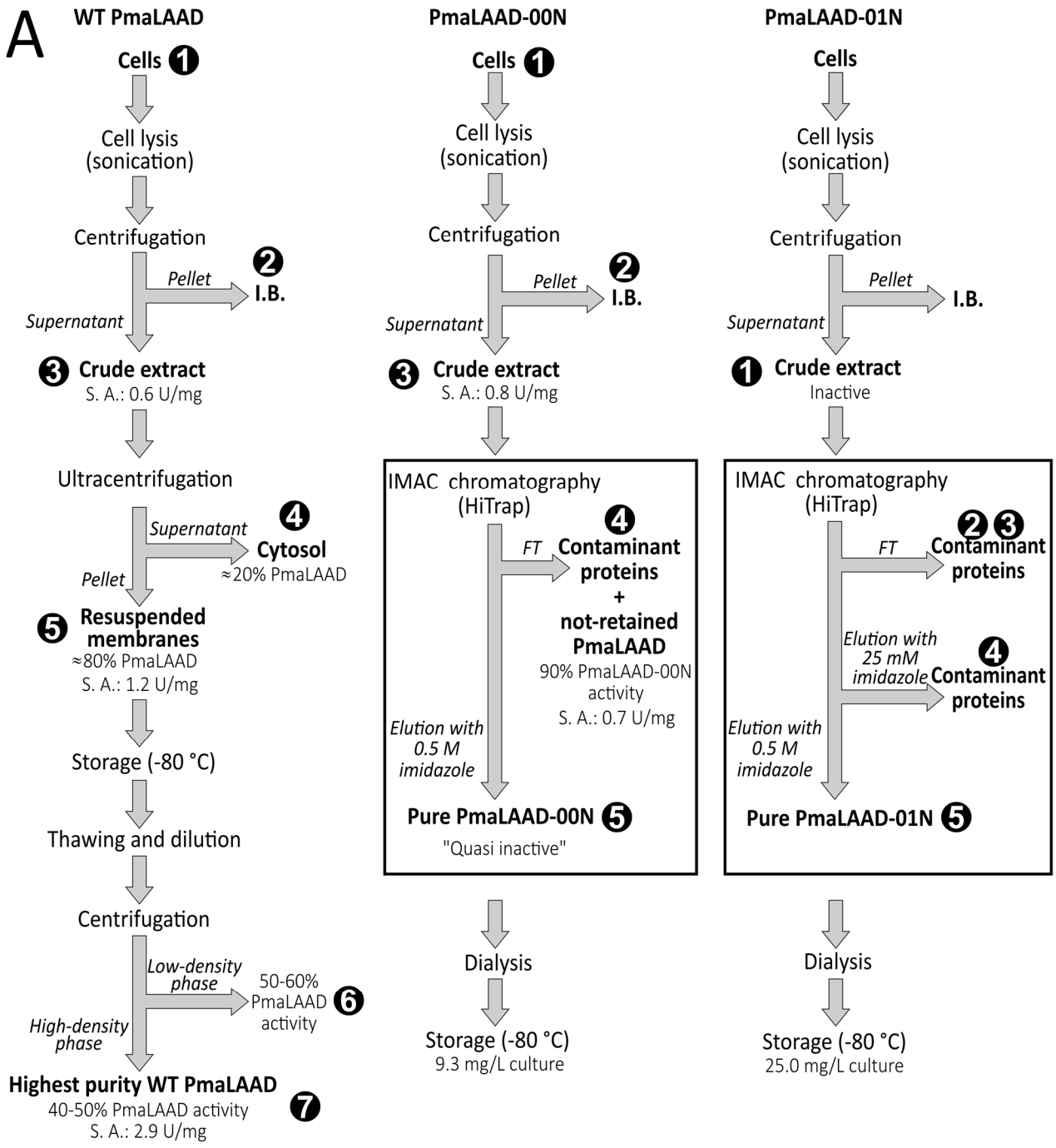
A
WT PmaLAAD
Cells ❶
Cell lysis (sonication)
Centrifugation
Pellet
❷ I.B.
Supernatant
❸ Crude extract
S. A.: 0.6 U/mg
Ultracentrifugation
Supernatant
❹ Cytosol
≈20% PmaLAAD
Pellet
❺ Resuspended membranes
≈80% PmaLAAD
S. A.: 1.2 U/mg
Storage (-80 °C)
Thawing and dilution
Centrifugation
Low-density phase
50-60% PmaLAAD activity ❻
High-density phase
Highest purity WT PmaLAAD
40-50% PmaLAAD activity
S. A.: 2.9 U/mg ❼
PmaLAAD-00N
Cells ❶
Cell lysis (sonication)
Centrifugation
Pellet
❷ I.B.
Supernatant
❸ Crude extract
S. A.: 0.8 U/mg
IMAC chromatography (HiTrap)
FT
❹ Contaminant proteins + not-retained PmaLAAD
90% PmaLAAD-00N activity
S. A.: 0.7 U/mg
Elution with 0.5 M imidazole
Pure PmaLAAD-00N ❺
"Quasi inactive"
Dialysis
Storage (-80 °C)
9.3 mg/L culture
PmaLAAD-01N
Cells
Cell lysis (sonication)
Centrifugation
Pellet
I.B.
Supernatant
❶ Crude extract
Inactive
IMAC chromatography (HiTrap)
FT
❷ ❸ Contaminant proteins
Elution with 25 mM imidazole
❹ Contaminant proteins
Elution with 0.5 M imidazole
Pure PmaLAAD-01N ❺
Dialysis
Storage (-80 °C)
25.0 mg/L culture
B
M 1 2 3 4 5 6 7
95 72 55 43 34 26
M 1 2 3 4 5
95 72 55 43 34 26
M 1 2 3 4 5
95 72 55 43 34 26

Figure 3

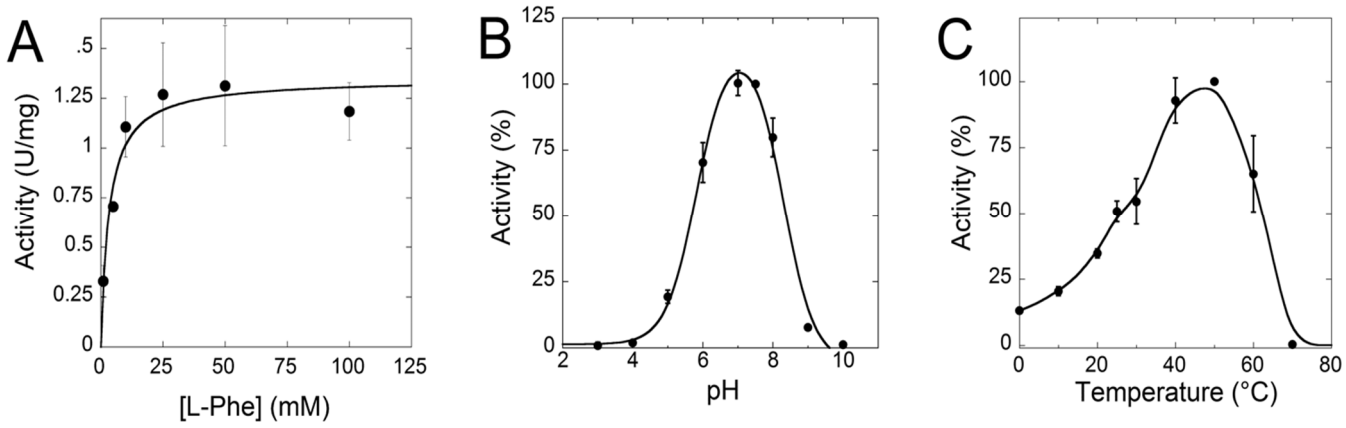
A
Activity (U/mg)
.5
1.25
1
0.75
0.5
0.25
0
0
25
50
75
100
125
[L-Phe] (mM)
B
Activity (%)
125
100
75
50
25
0
2
4
6
8
10
pH
C
Activity (%)
100
75
50
25
0
0
20
40
60
80
Temperature (°C)

Figure 4

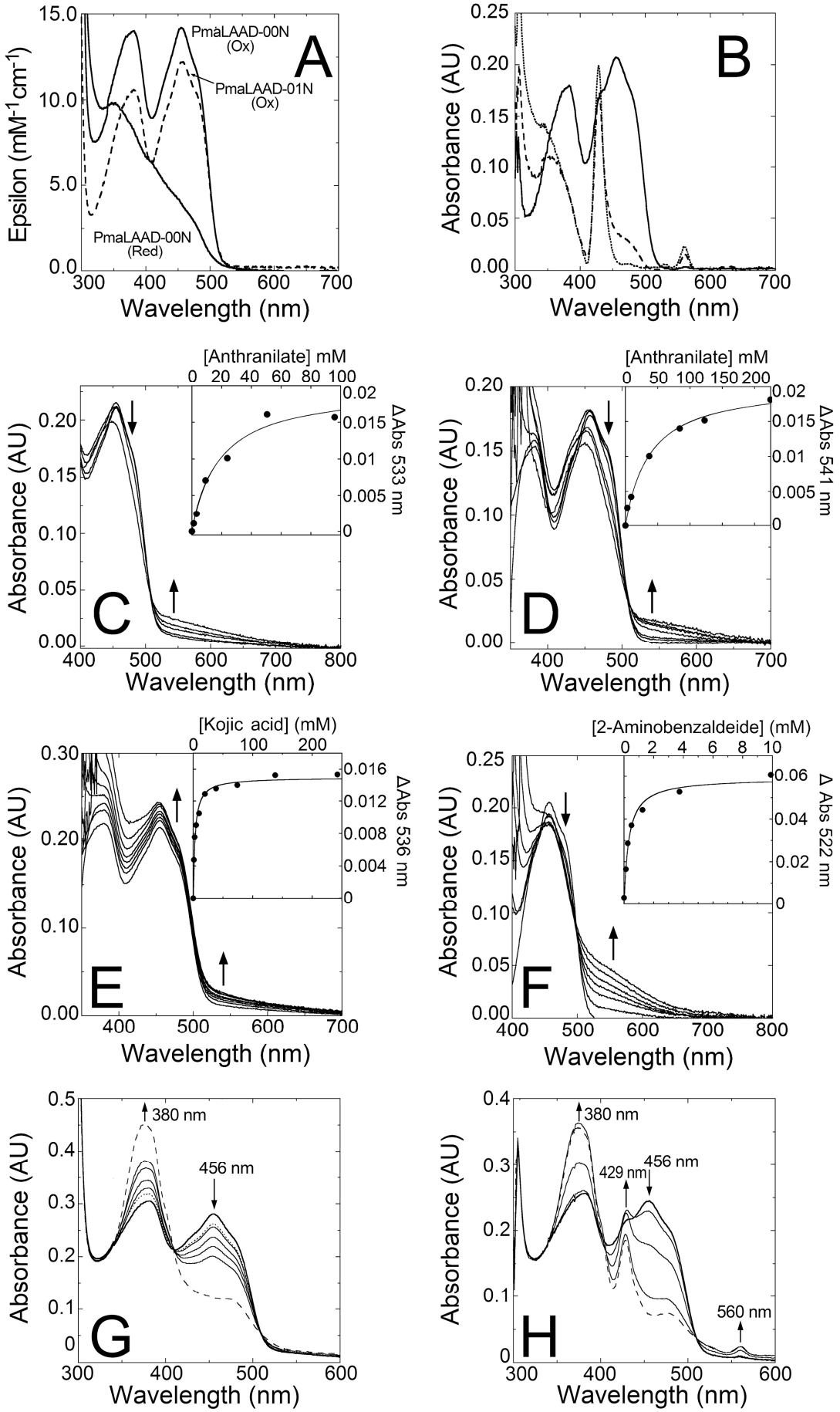
A
PmaLAAD-00N (Ox)
PmaLAAD-01N (Ox)
PmaLAAD-00N (Red)
Epsilon (mM-1cm-1)
Wavelength (nm)
B
Absorbance (AU)
Wavelength (nm)
C
[Anthranilate] mM
0 20 40 60 80 100
ΔAbs 533 nm
Absorbance (AU)
Wavelength (nm)
D
[Anthranilate] mM
0 50 100 150 200
ΔAbs 541 nm
Absorbance (AU)
Wavelength (nm)
E
[Kojic acid] (mM)
0 100 200
ΔAbs 536 nm
Absorbance (AU)
Wavelength (nm)
F
[2-Aminobenzaldeide] (mM)
0 2 4 6 8 10
Δ Abs 522 nm
Absorbance (AU)
Wavelength (nm)
G
380 nm
456 nm
Absorbance (AU)
Wavelength (nm)
H
380 nm
429 nm
456 nm
560 nm
Absorbance (AU)
Wavelength (nm)

Figure 5

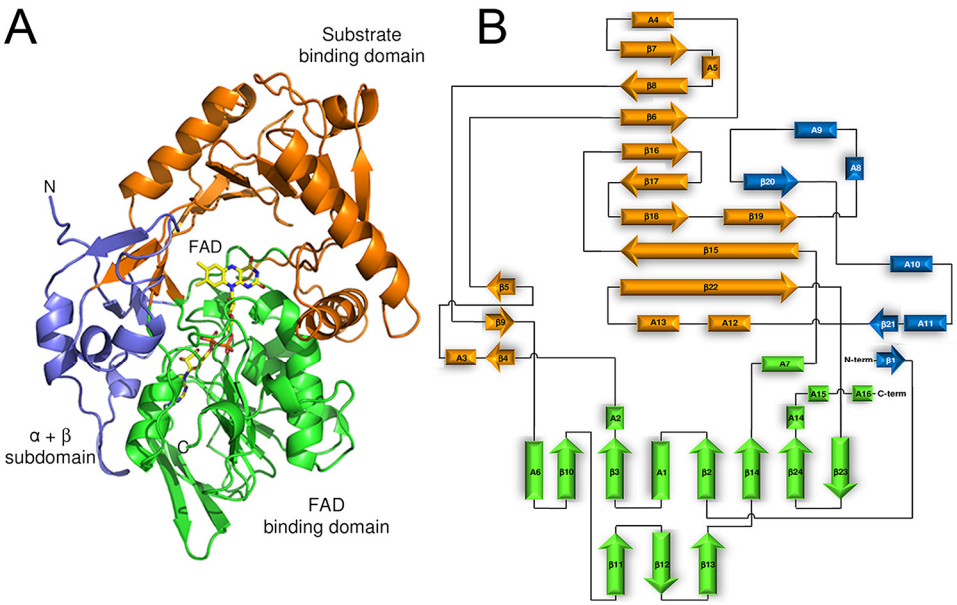

C


```
PmaLAAD-01N     MVRRDGKFVESKSRALFVESTEGALPSESDVVIIGGGIQGIMTAINLAER-G-MSVTILEKGEV   89
PmaLAAD-01N-A   MVRRDGKFVESKSRALFVESTEGALPSESDVVIIGGGIQGIMTAINLAER-G-MSVTILEKGEV   89
1Y56            ------------------------LPEKSEIVVIGGGIVGVTIAHELAKR-G-EEVTVIEKRFI   39
1C0I            ----------------------LMMHSQKRVVVLGSGVIGLSSALILARK-G-YSVHILARDLP  1038
3ADA            -------------EHPEFLWNNPEPKKSYDVVIVGGGGHGLATAYYLAKNHGITNVAVLEKGWL   56
2GAG            ---------DLLPEHPEFLWANPEPKKSYDAIIVGGGGHGLATAYFLAKNHGITNVAVLEKGWL   57
```


```
PmaLAAD-01N     -----AGEQSGRAYSQIISYQTS---PEIFPLHHYGKILWRGMNEKIGADTSYRTQ-GRVEALA   144
PmaLAAD-01N-A   -----AGEQSGRAYSQIISYQTS---PEIFPLHHYGKILWRGMNEKIGADTSYRTQ-GRVEALA   144
1Y56            -----GSGSTFRCGTGIRQQFND---EANVRVMKRSVELWKKYSEEYG--FSFKQT-GYLFLLY    92
1C0I            EDVSSQTFASPWAGANWTPFMTLTDGPRQAKWEESTFKKWVELVPTG----HAMWLKGTRRFAQ  1098
3ADA            -----AGGNMARNTTIIRSNYLW---DESAGIYEKSLKLWEELPEELEYDFLFSQR-GVLNLAH   111
2GAG            -----AGGNMARNTTIIRSNYLW---DESAGIYEKSLKLWEQLPEDLEYDFLFSQR-GVLNLAH   112
```


```
PmaLAAD-01N     DEKALDRAQEWIKTAKETAGFDVPLNTRIIKGEELSNRLVGAQTP------WTVAAFEEDSGSV   202
PmaLAAD-01N-A   DEKALDRAQEWIKTAKETAGFDVPLNTRIIKGEELSNRLVGAQTP------WTVAAFEEDSGSV   202
1Y56            DDEEVKTFKRNIEIQNKFG-----VPTKLITPEEAKEIVPLLDIS-----EVIAASWNPTDGKA   146
1C0I            NEDGLLGHWYKDITP----------NYRPLPSSECPPGA--------------IGVTY-DTLSV  1137
3ADA            TLGDVRESIRRVEANKFNG-----VDAEWLTPEQVKEVCPIINTGDNIRYPVMGATYQPRAGIA   170
2GAG            TLGDVRESVRRVEANKLNG-----VDAEWLDPSQVKEACPIINTSDDIRYPVMGATWQPRAGIA   171
```


```
PmaLAAD-01N     DPETGTPTLARYAKQIGVKIYTHCAVRGIETAGGKISDVVTEKGAIRTSNVVLAGGIWSRLFMG   266
PmaLAAD-01N-A   DPETGTPTLARYAKQIGVKIYTHCAVRGIETAGGKISDVVTEKGAIRTSNVVLAGGIWSRLFMG   266
1Y56            DPFEATTAFAVKAKEYGAKLLEYTEVKGFLIENNEIKGVKTNKGIIKTGIVVNATNAWANLINA   210
1C0I            HAPKYCQYLARELQKLGATFERRTVTSLEQA-------------FDGADLVVNATGLGAKSIA-  1187
3ADA            KHDHVAWAFARKANEMGVDIIQNCEVTGFLKDGEKVTGVKTTRGTILAGKVALAGAGHSSVLAE   234
2GAG            KHDHVAWAFARKANEMGVDIIQNCEVTGFIKDGEKVTGVKTTRGTIHAGKVALAGAGHSSVLAE   235
```


```
PmaLAAD-01N     NMGV--DLPTLNVYLSQQRVS-GVPGAPRGNVHLPN----GIHFREQADGTYAVAPRIFTSSIV   323
PmaLAAD-01N-A   NMGV--DLPTLNVYLSQQRVS-GVPGAPRGNVHLPN----GIHFREQADGTYAVAPRIFTSSIV   323
1Y56            MAGIKTKIPIEPYKHQAVITQPIKRGTINPMVISFKYG--HAYLTQTFHGGIIGGIGYEIG---   269
1C0I            --GI-DDQAAEPIRGQTVLVK---SPCKR-CTMDSSDPASPAYIIPRPGGEVICGGTYGVG---  1241
3ADA            LAGF--ELPIQSHPLQALVSELFEP-VHPTVVMSNHI---HVYVSQAHKGELVMGAGIDSY---   289
2GAG            MAGF--ELPIQSHPLQALVSELFEP-VHPTVVMSNHI---HVYVSQAHKGELVMGAGIDSY---   290
```


```
PmaLAAD-01N     KDSFLLGPKFMHLLGGGELPLEFSIGEDLFNSFKMPTSWKLDEKSPFEQYRIATATQNTEHLDA   387
PmaLAAD-01N-A   KDSFLLGPKFMHLLGGGELPLEFSIGEDLFNSFKMPTSWKLDEKSPFEQYRIATATQNTEHLDA   387
1Y56            ------------------------------------------------------PTYDLTPTYEFLRE   283
1C0I            ----------------------------------------------------DWDLSVNPETVQR  1254
3ADA            ---------------------------------------------------NGYGQRGAFHVIEE   303
2GAG            ---------------------------------------------------NGYGQRGAFHVIQE   304
```


```
PmaLAAD-01N     VFQRMKTEFPVFEKS------QIVERWGAVVSPTFDELPIISEVKE-------------------   427
PmaLAAD-01N-A   VFQRMKTEFPVFEKS------QIVERWGAVVSPTFDELPIISEVKE-------------------   427
1Y56            VSYYFTKIIPALKNL------LILRTWAGYYAKTPDSNPAIGRIEE-------------------   323
1C0I            ILKHCLRLDPTISSDGTIEGIEVLRHNVGLRPARRG-GPRVEAERIVLPLDRTKSPLSLGRGSA  1317
3ADA            QMAAAVELFPIFARA------HVLRTWGGIVDTTMDASPIISKTPI-------------------   343
2GAG            QMAAAVELFPIFARA------HVLRTWGGIVDTTMDASPIISKTPI-------------------   344
```


```
PmaLAAD-01N     ------YPGLVINTATV-WGMTEGPAAGEVTADIVTGKKPVIDPTPFSLDRFKK              474
PmaLAAD-01N-A   ------YPGLVINTATV-WGMTEGPAAGEVTADIVTGKKPVIDPTPFSLDRFKK              474
1Y56            ------LNDYYIAAGFSGHGFMMAPAVGEMVAELITKGKTKLPVEWYDPYRFERGELR          375
1C0I            RAAKEKEVTLVHAYGFSSAGYQQSWGAAEDVAQLVDEAFQRYHG                      1361
3ADA            -------QNLYVNCGWGTGGFKGTPGAGYTLAHTIAHDEPHKLNAPFALERFETGHLIDEHGAAAV  402
2GAG            -------QNLYVNCGWGTGGFKGTPGAGFTLAHTIANDEPHELNKPFSLERFETGHLIDEHGAAAV  405
```

Figure 6

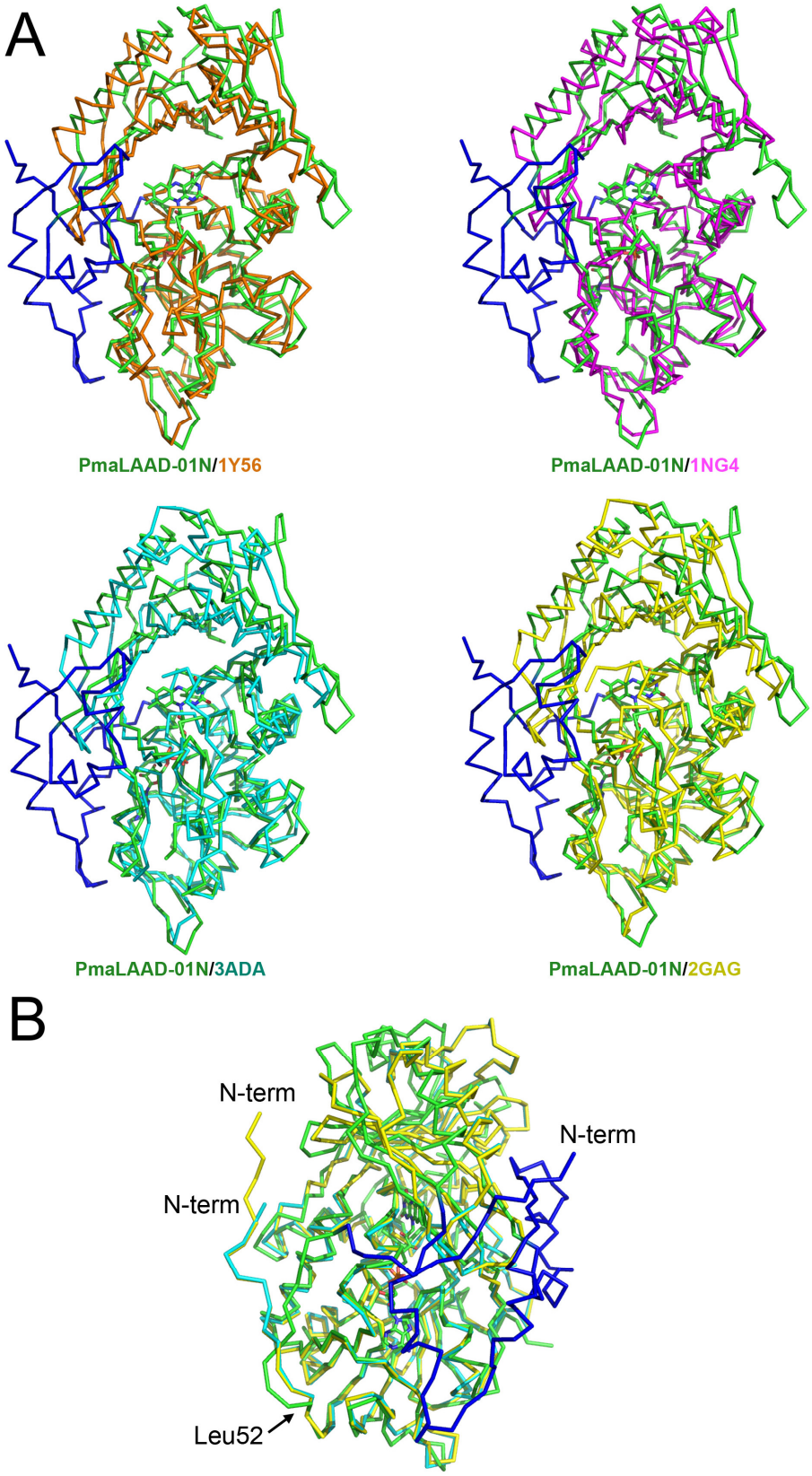
A
PmaLAAD-01N/1Y56
PmaLAAD-01N/1NG4
PmaLAAD-01N/3ADA
PmaLAAD-01N/2GAG
B
N-term
N-term
N-term
Leu52

Figure 7

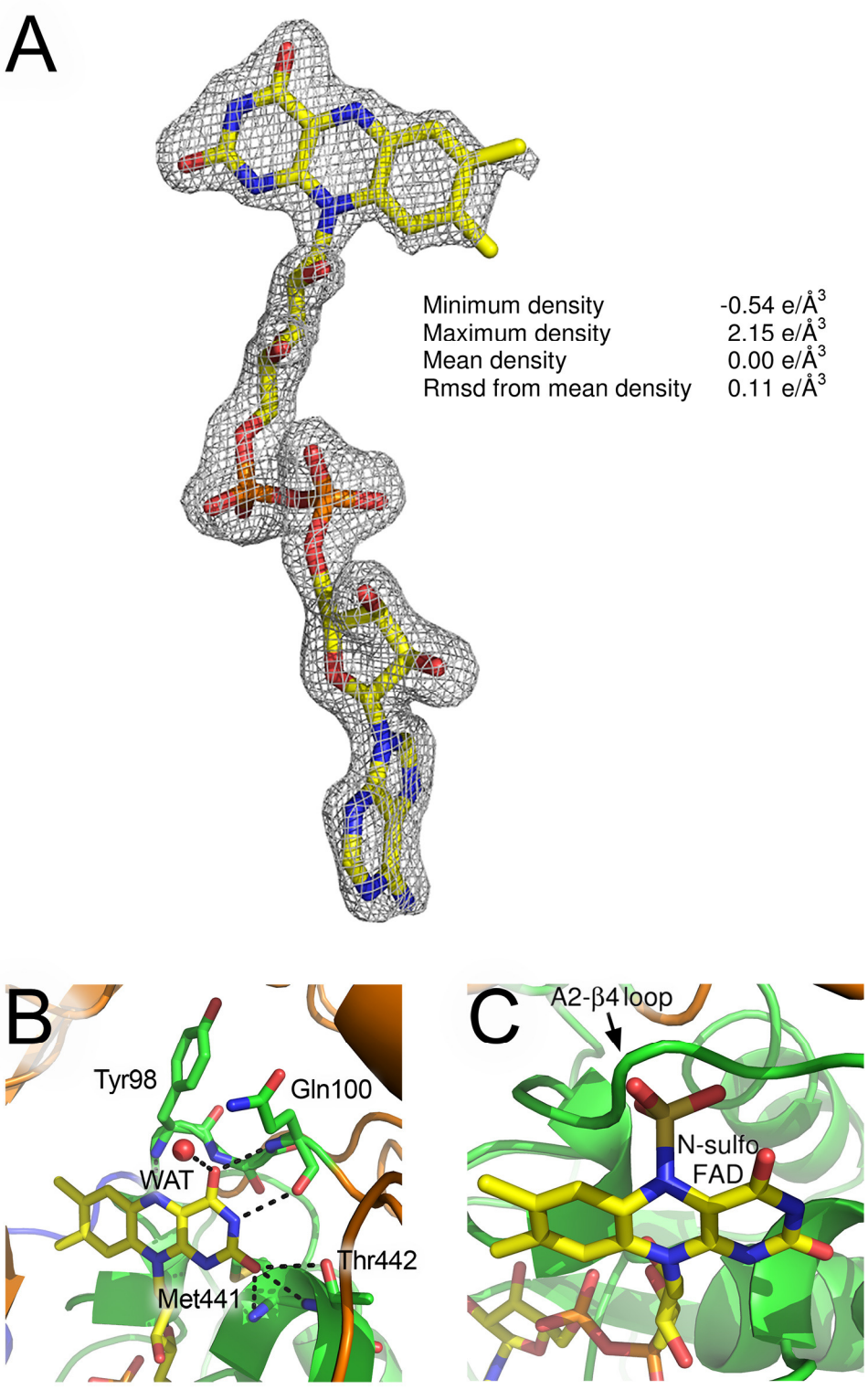
A
Minimum density -0.54 e/Å3
Maximum density 2.15 e/Å3
Mean density 0.00 e/Å3
Rmsd from mean density 0.11 e/Å3
B
Tyr98
Gln100
WAT
Thr442
Met441
C
A2-β4 loop
N-sulfo
FAD

Figure 8

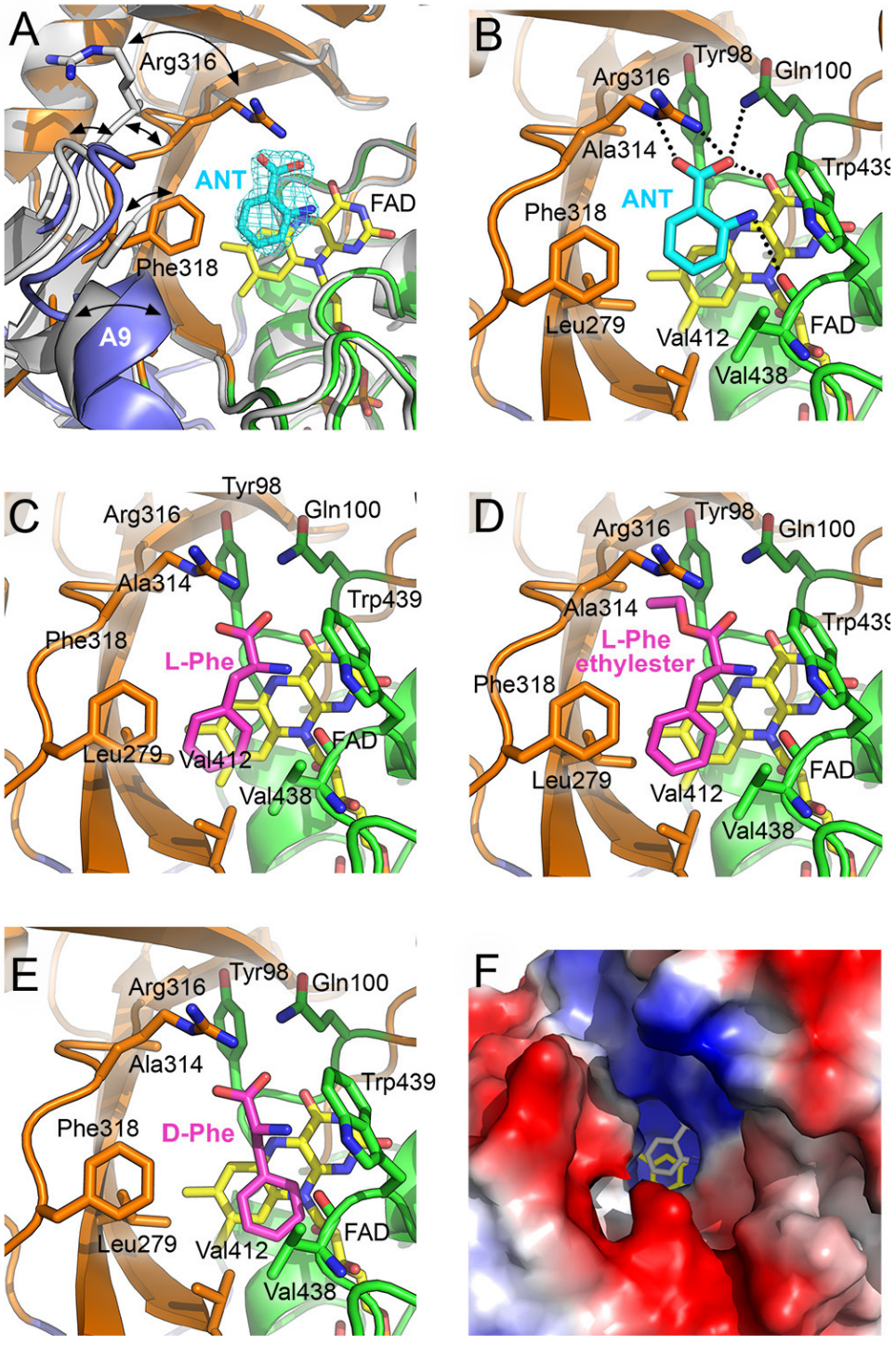
A
Arg316
ANT
FAD
Phe318
A9
B
Tyr98
Gln100
Arg316
Ala314
Trp439
ANT
Phe318
Leu279
Val412
FAD
Val438
C
Tyr98
Arg316
Gln100
Ala314
Trp439
Phe318
L-Phe
FAD
Leu279
Val412
Val438
D
Arg316
Tyr98
Gln100
Ala314
Trp439
L-Phe
ethylester
Phe318
Leu279
Val412
FAD
Val438
E
Arg316
Tyr98
Gln100
Ala314
Trp439
Phe318
D-Phe
Leu279
Val412
FAD
Val438
F

Figure 9

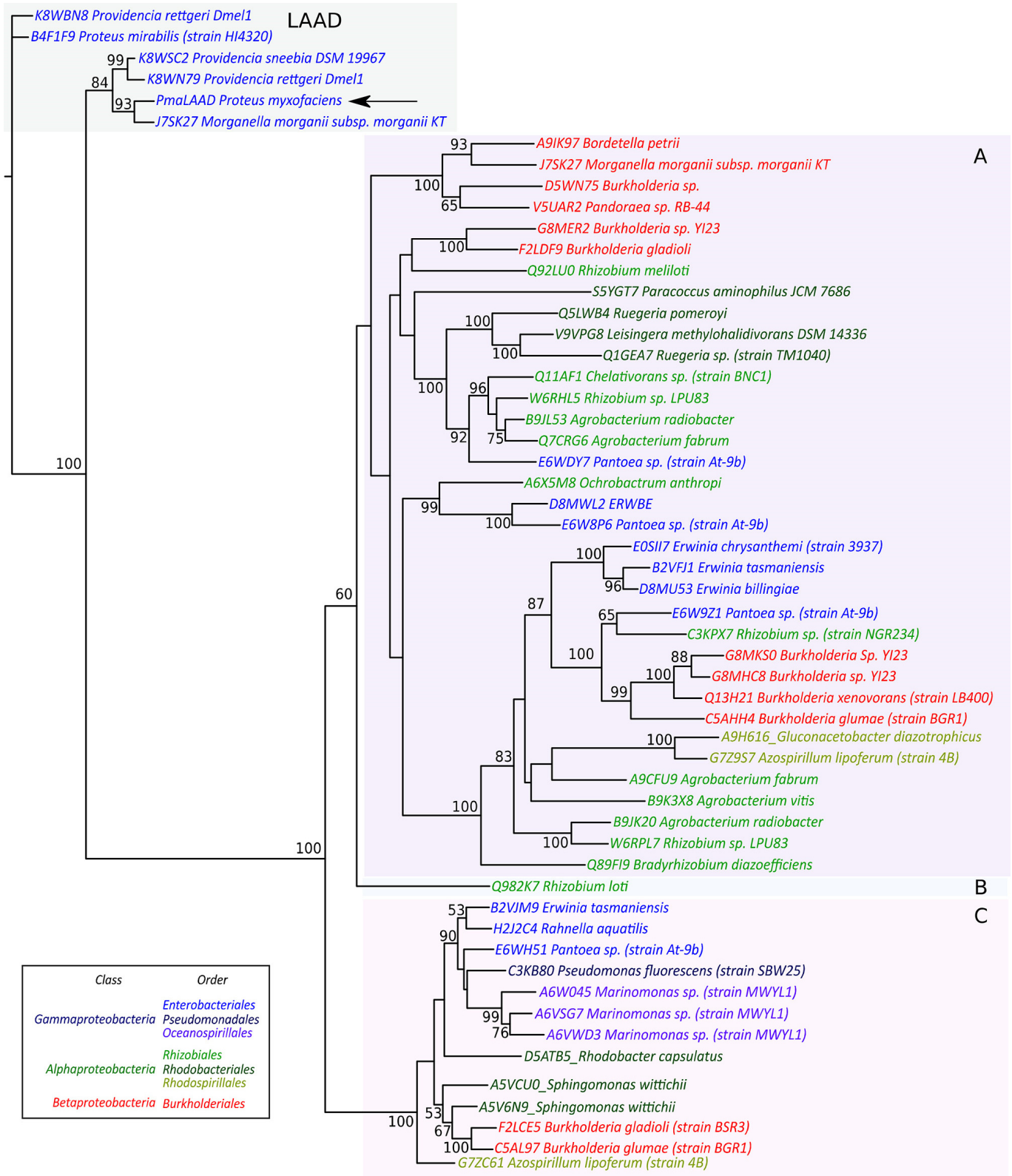
LAAD
K8WBN8 Providencia rettgeri Dmel1
B4F1F9 Proteus mirabilis (strain HI4320)
K8WSC2 Providencia sneebia DSM 19967
K8WN79 Providencia rettgeri Dmel1
PmaLAAD Proteus myxofaciens
J7SK27 Morganella morganii subsp. morganii KT
A
A9IK97 Bordetella petrii
J7SK27 Morganella morganii subsp. morganii KT
D5WN75 Burkholderia sp.
V5UAR2 Pandoraea sp. RB-44
G8MER2 Burkholderia sp. YI23
F2LDF9 Burkholderia gladioli
Q92LU0 Rhizobium meliloti
S5YGT7 Paracoccus aminophilus JCM 7686
Q5LWB4 Ruegeria pomeroyi
V9VPG8 Leisingera methylohalidivorans DSM 14336
Q1GEA7 Ruegeria sp. (strain TM1040)
Q11AF1 Chelativorans sp. (strain BNC1)
W6RHL5 Rhizobium sp. LPU83
B9JL53 Agrobacterium radiobacter
Q7CRG6 Agrobacterium fabrum
E6WDY7 Pantoea sp. (strain At-9b)
A6X5M8 Ochrobactrum anthropi
D8MWL2 ERWBE
E6W8P6 Pantoea sp. (strain At-9b)
E0SII7 Erwinia chrysanthemi (strain 3937)
B2VFJ1 Erwinia tasmaniensis
D8MU53 Erwinia billingiae
E6W9Z1 Pantoea sp. (strain At-9b)
C3KPX7 Rhizobium sp. (strain NGR234)
G8MKS0 Burkholderia Sp. YI23
G8MHC8 Burkholderia sp. YI23
Q13H21 Burkholderia xenovorans (strain LB400)
C5AHH4 Burkholderia glumae (strain BGR1)
A9H616_Gluconacetobacter diazotrophicus
G7Z9S7 Azospirillum lipoferum (strain 4B)
A9CFU9 Agrobacterium fabrum
B9K3X8 Agrobacterium vitis
B9JK20 Agrobacterium radiobacter
W6RPL7 Rhizobium sp. LPU83
Q89FI9 Bradyrhizobium diazoefficiens
B
Q982K7 Rhizobium loti
C
B2VJM9 Erwinia tasmaniensis
H2J2C4 Rahnella aquatilis
E6WH51 Pantoea sp. (strain At-9b)
C3KB80 Pseudomonas fluorescens (strain SBW25)
A6W045 Marinomonas sp. (strain MWYL1)
A6VSG7 Marinomonas sp. (strain MWYL1)
A6VWD3 Marinomonas sp. (strain MWYL1)
D5ATB5_Rhodobacter capsulatus
A5VCU0_Sphingomonas wittichii
A5V6N9_Sphingomonas wittichii
F2LCE5 Burkholderia gladioli (strain BSR3)
C5AL97 Burkholderia glumae (strain BGR1)
G7ZC61 Azospirillum lipoferum (strain 4B)
Class
Order
Gammaproteobacteria
Enterobacteriales
Pseudomonadales
Oceanospirillales
Alphaproteobacteria
Rhizobiales
Rhodobacteriales
Rhodospirillales
Betaproteobacteria
Burkholderiales